UNIVERSITAT ROVIRA i VIRGILI
Dept. de Química Analítica
i Química Orgànica

SINTCARB
Stereoselective Organic Synthesis
Carbohydrate Chemistry

# Synthesis of Ceramide PR280 Analogues Bearing Basic *N*-Acyl Modifications for Targeted Des1 Inhibition

**Final Degree Project**

**Adrián Jiménez Jerez**

**Tutors:**

**Prof. María Isabel Matheu Malpartida**

**Dr. María Yolanda Díaz Giménez**

## Agradecimientos/ Acknowledgements

Me gustaría comenzar dando las gracias a la profesora Maribel Matheu y a la doctora Yolanda Díaz, las tutoras de este trabajo. Gracias por despertar mi ilusión permitiéndome trabajar y formar parte en este proyecto tan interesante, además de los consejos y valiosas enseñanzas fruto de vuestra experiencia. Muchas gracias por ser parte de mi primera etapa como investigador y formarme con tanta calidad.

Quiero agradecer a quien primero me formó en este grupo de investigación durante mis primeras prácticas cuándo yo no tenía ni idea de trabajar en un laboratorio, Pablo, por haberme asentado las bases de lo que significa trabajar con rigurosidad y adecuadamente en un laboratorio, de una manera muy agradable y positiva que despiertan las ganas de mejorar.
Este trabajo no podría haber sido posible sin la organización y dirección de quien me ha estado guiando y formando en este camino durante estos últimos meses, Eric, quien ha sido mi supervisor y consejero. Gracias a la experiencia y calidad de los dos he podido mejorar a un ritmo mucho más rápido.

Me gustaría agradecer también a cada integrante de SINTCARB. Gracias por ayudarme en cualquier adversidad y hacer del ambiente de trabajo un entorno cálido donde uno se siente a gusto.
En especial me gustaría agradecer a Dahiana, quien ha sido mi compañera de vitrina durante este trabajo. Muchas gracias por aguantarme, por ofrecerme tanta ayuda y por entretener mis columnas con conversaciones tan interesantes fruto de tus filosofías tan únicas y espontaneas, y por todos los momentos vividos fuera del laboratorio, me llevo a una persona increíble de esta experiencia. También quiero agradecer a Teresa. Los dos empezamos de 0 juntos, y me llena de orgullo ver el camino que hemos recorrido y lo mucho que hemos mejorado los dos. Has hecho de esta experiencia una mucho más fácil y agradable, muchas gracias por tantas risas, por comprenderme tanto y por ser mi símil en esta etapa, empezaste siendo mi compañera y ahora eres una amiga en la que confío plenamente.

Lauren, muchísimas gracias. Desde el primer momento vi en ti una persona increíble, muy similar a mí. El tiempo contigo y el amor que me has dado me han dado fuerzas, ánimos, y una visión con mucha más perspectiva que me han permitido avanzar mucho en esta etapa. Gracias por hacer mis problemas insignificantes y por hacerme mejor persona, por quererme y por escucharme cuando más lo necesito, me das vida. Te quiero.

Por último, quiero agradecer a mi familia, a quienes dedico este trabajo.
A mis abuelos y a mi tío, gracias por tanta ayuda desinteresada y tanto amor, sois luz y motivación para mí, me habéis construido desde los valores más bonitos.
A mis padres, gracias por no soltarme nunca, por cuidarme tanto y por superar cada adversidad conmigo, es gracias a vosotros que me puedo graduar después de un camino que no ha sido fácil pero que con vosotros al lado lo ha parecido. Gracias por hacerme ser quien soy.
A mi hermana. Qué agradecido me siento de tener la relación que tengo contigo. Qué bonito es tener a una persona que te apoya en todo para siempre, que sabes que pase lo que pase siempre va a estar ahí para ayudarte. Tu apoyo y la confianza que siempre has tenido en mi cuando ni yo la tenía han sido vitales durante toda la carrera. Estoy entusiasmado de seguir compartiendo logros junto a ti, te quiero hermanita.

## Table of contents

## Abbreviations and acronyms

| | | |
|---|---|---|
| **A** | **Ac** | Acetate |
| | **AI** | Artificial intelligence |
| **B** | **Boc** | *tert*-Butyloxycarbonyl |
| | **Bu** | Buthyl |
| **C** | **CDase** | Ceramidase |
| | **Cer** | Ceramide |
| | **CerS** | Sphingosine *N*-acetyltransferase |
| | **COSY** | Proton homonuclear correlation spectroscopy |
| | **CSIC** | Higher Council for Scientific Research |
| **D** | **3D** | Three dimensional |
| | **DCC** | Dicyclohexylcarbodiimide |
| | **Des1** | Dihydroceramide desaturase 1 |
| | **dhCer** | Dihydroceramide |
| | **dhSM** | Dihydrosphyngomyelin |
| | **DIPEA** | *N,N*-Diisopropylethylamine |
| | **DMF** | Dimethylformamide |
| | **DMSO** | Dimethyl sulfoxide |
| **E** | **EDC** | 1-ethyl-3-(3-dimethylaminopropyl)carbodiimide |
| | **equiv.** | Equivalent(s) |
| **H** | **HATU** | Hexafluorophosphate azabenzotriazole tetramethyl uranium |
| | **HBTU** | Hexafluorophosphate benzotriazole tetramethyl uranium |
| | **HMPA** | Hexamethylphosphoramide |
| | **h** | Hour(s) |
| | **HRMS** | High-resolution Mass spectrometry |
| **I** | **$IC_{50}$** | Half maximal inhibitory concentration |
| | **ICREA** | Catalan Institution for Research and Advanced Studies |
| | **IQAC** | Institute of Advanced Chemistry of Catalonia |
| | **IR** | Infrared |
| **K** | **KSDR** | 3-Ketodihydrosphingosine Short-chain Dehydrogenase |
| **M** | **M** | Molar |

| | | |
|---|---|---|
| | **min** | Minute(s) |
| **N** | **NMP** | *N*-Methyl-2-pyrrolidine |
| | **NMR** | Nuclear Magnetic Resonance |
| **O** | **Oat** | 7-azabenzotriazole |
| | **o/n** | Overnight |
| **P** | **pLDDT** | Predicted Local Distance Difference Test |
| | **ppm** | Parts per million |
| | **PyBOP** | **(**benzotriazol-1-yloxy)tripyrrolidinophosphonium hexafluorophosphate |
| **R** | **R** | Substituent |
| | **r.t.** | Room temperature |
| **S** | **S1P** | Sphingosine-1-phosphate |
| | **SM** | Sphyngomyelin |
| | **SphK** | Sphingosine Kinase |
| | **SPP** | S1P phosphatases |
| | **SPT** | Serine palmitoyl-CoA transferase |
| **T** | **THF** | Tetrahydrofuran |
| | **TLC** | Thin layer chromatography |
| | **TMS** | Trimethylsilyl |

# Abstract


## English

Dihydroceramide desaturase 1 (Des1) plays a key role in sphingolipid biosynthesis. Its inhibition leads to dihydroceramide (dhCer) accumulation—inducing autophagy—preventing ceramide (Cer) formation and its pro-tumor metabolite sphingosine-1-phosphate (S1P), making Des1 a potential anticancer target. Previous work by SINTCARB group identified **PR280**, a ceramide incorporating a cyclopropenone moiety, as a potent Des1 inhibitor.

This project aimed to develop three *N*-acylated **PR280** analogues bearing basic functional groups, selected through virtual screening and docking predictions. The synthetic route included scaffold protection, stereoselective addition to (*S*)-Garner's aldehyde, global deprotection, and final *N*-acylation. Conditions were optimized for each step.

The final compounds—**PR280-1**, **PR280-3**, and **PR280-7**—were fully characterized by NMR, HRMS, and IR. Overall isolated yields were 26 %, 33 %, and 13 % across six, five, and seven-step syntheses, respectively. These novel analogues represent promising candidates for future Des1 inhibitor development.

## Spanish

La dihidroceramida desaturasa 1 (Des1) desempeña un papel fundamental en la biosíntesis de esfingolípidos. Su inhibición provoca la acumulación de dihidroceramida (dhCer), lo que induce procesos de autofagia, e impide la formación de ceramida (Cer) y, por tanto, de su metabolito pro-tumoral, la esfingosina-1-fosfato (S1P). Por ello, Des1 se perfila como una diana terapéutica de gran interés en el contexto de tratamiento del cáncer. En investigaciones previas, llevadas a cabo en el grupo de investigación SINTCARB, se identificó a **PR280**, una ceramida que incorpora un motivo ciclopropenona, como un potente inhibidor de Des1.

El presente trabajo se centró en el desarrollo de tres análogos *N*-acilados de **PR280** con grupos funcionales básicos, seleccionados mediante cribado virtual y estudios de acoplamiento molecular. La ruta sintética incluye la protección de grupos funcionales sensibles, una adición estereoselectiva al aldehído de Garner (*S*), desprotección global y acilación final, optimizando las condiciones en cada etapa.

Los compuestos finales—**PR280-1**, **PR280-3** y **PR280-7**—se caracterizaron completamente mediante RMN, HRMS e IR, y se obtuvieron con rendimientos globales del 26 %, 33 % y 13 %, respectivamente, en rutas sintéticas de seis, cinco y siete etapas. Estos nuevos análogos representan estructuras prometedoras para el desarrollo futuro de inhibidores de Des1.

# 1. Introduction

## 1.1. Bioactive sphingolipids

Lipids play diverse and essential roles in cellular function, contributing not only to energy regulation but also to structural integrity. Among them, **bioactive lipids** stand out as key regulators within cellular signaling networks. Their levels fluctuate in response to specific stimuli, reflecting their involvement in dynamic regulatory processes. Owing to their diversity and abundance, bioactive lipids are integral to nearly all major cellular pathways.

**Sphingolipids** represent one of the most prominent classes of bioactive lipids in eukaryotic cells. These compounds were first isolated from brain tissue in the late 19th century by Johann Thudicum.[1] Initial research focused on elucidating their chemical structure, particularly that of sphingosine, a primary sphingoid base that serves as a fundamental building block for all sphingolipids.

It was not until the 1980s that the bioactive functions of key sphingolipids—namely **sphingosine**, **ceramide**, and **sphingosine-1-phosphate (S1P)**—were fully recognized. These studies revealed their critical roles in the regulation of cell growth, differentiation, and apoptosis, sparking intense interest in the biological functions of sphingolipids.[1]

Structurally, sphingolipids are characterized by their **amphipathic nature**. They possess a polar (hydrophilic) head group composed of a 2-amino-1,3-diol backbone, and a non-polar (hydrophobic) long-chain alkyl tail. This dual character underpins their functional versatility within cellular membranes and signaling environments.

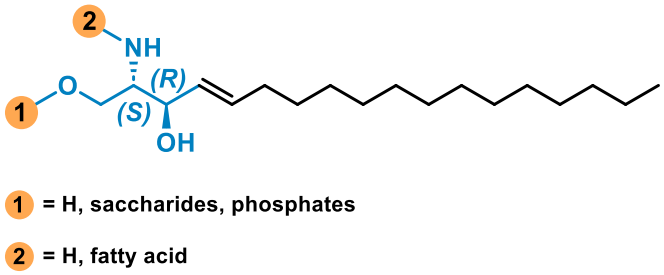


***Figure 1**: general structure of most sphingolipids.*

The core structure of sphingolipids—excluding potential substituents at the 2-amino and 1-hydroxyl positions—consists of an 18-23 carbon backbone featuring in most of the cases a *trans-configured* double bond at carbon 4. The chiral centers at positions 2 and 3 in the polar head adopt an *anti*-diastereospecific configuration with the absolute configuration being *(2S,3R)*.

## 1.2. Enzymatic regulation of sphingolipid metabolism: sphingolipid rheostat and *de novo* synthesis of sphingolipids

Bioactive sphingolipids are tightly regulated by a variety of enzymes operating across multiple metabolic pathways. The dynamic balance between pro-apoptotic ceramide and sphingosine, and the pro-survival metabolite sphingosine-1-phosphate (S1P) is referred to as the **sphingolipid rheostat** (Scheme 1), and collectively regulates cell fate. Ceramide can be deacylated by ceramidases to form sphingosine, which is then phosphorylated by sphingosine kinases (SphK1 and SphK2) to generate S1P. Conversely, S1P can be dephosphorylated back to sphingosine by S1P phosphatases (SPP) or irreversibly degraded

[1] Thudichum, J. L. W. *A Treatise on the Chemical Constitution of the Brain*; Archon Books: New York, **1962**.

by S1P lyase. Therefore, ceramide is a central bioactive sphingolipid involved in critical cellular regulatory processes. Thus, ceramide promotes apoptosis, quiescence and senescence,[2] all of which serve as protective mechanisms against oncogenic transformation by eliminating or arresting damaged cells. In contrast, S1P exerts pro-survival effects by inhibiting apoptosis and promoting angiogenesis, thereby facilitating tumor growth and metastasis through enhanced nutrient and oxygen supply.[3] The balance between ceramide and S1P is tightly regulated by specific enzymes, and targeted modulation of this pathway can decisively influence whether a cell survives or undergoes programmed death.[4] As such, the sphingolipid rheostat represents a promising therapeutic target in cancer and other diseases characterized by dysregulated cell survival.

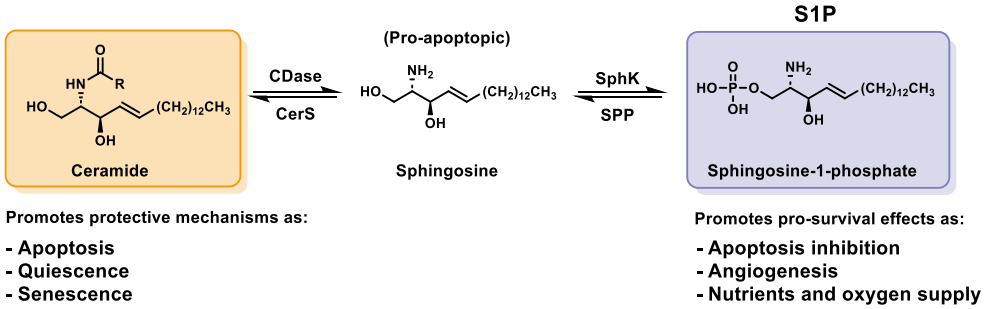


***Scheme 1**: Sphingolipid rheostat.*

Another primary mechanism of enzymatic regulation involves the ***de novo* synthesis of sphingolipids**:

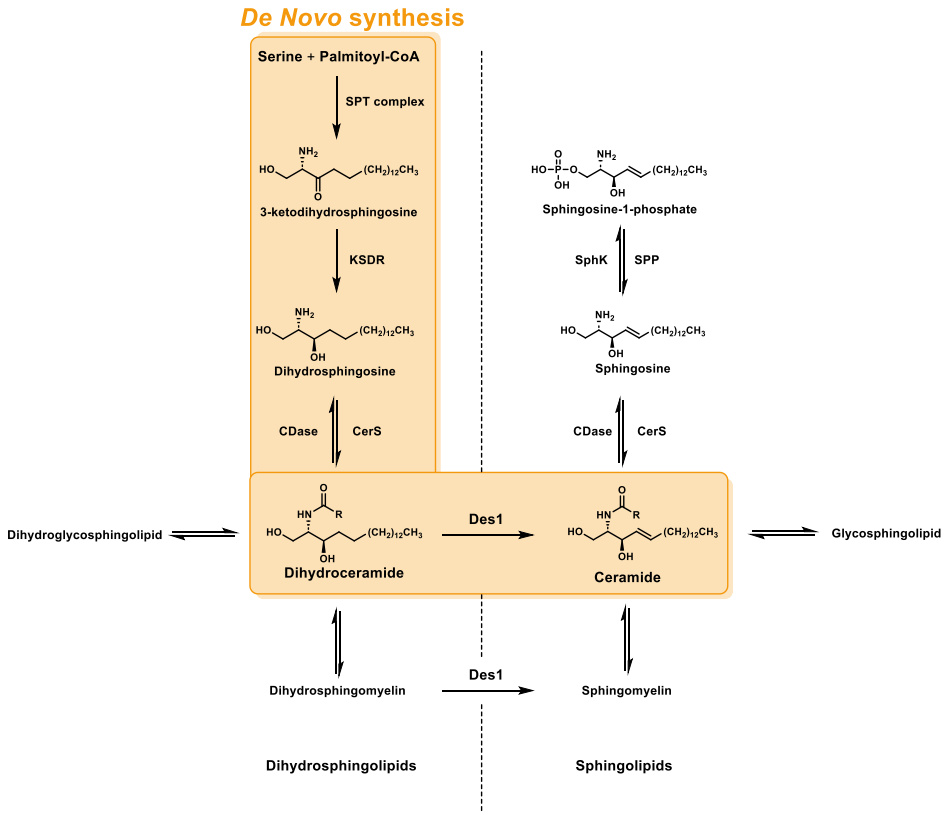


***Scheme 2**: De novo synthesis and global metabolic pathway of sphingolipids.*

[2] Obeid, L.M.; Linardic, C.M.; Karolak, L.A.; Hannun, Y.A. *Science* **1993**, *259*, 1769-1771.
[3] Pulkoski-Gross, M. J.; Donaldson, J. C.; Obedi, L. M. *Crit. Rev. Biochem. Mol. Biol*. **2015**, *50*, 298-313.
[4] Morad, S. A.; Cabot, M. C. *Nat. Rev. Cancer* **2013**, *13*, 51–65.

*De novo* synthesis (Scheme 2) is the metabolic pathway by which cells generate sphingolipid molecules from simple precursors. This metabolic pathway begins with the condensation of palmitoyl-CoA and serine, catalyzed by serine palmitoyltransferase (SPT), forming 3-ketodihydrosphingosine. Dihydrosphingosine undergoes *N*-acylation by (dihydro)ceramide synthases (CerS), incorporating a fatty acyl-chain to produce dihydroceramide. Subsequently, dihydroceramide is desaturated by dihydroceramide desaturase 1 (Des1) to form ceramide.

### 1.3. Dihydroceramides

Early studies on dihydroceramide (dhCer) suggested it was biologically inert in lipid metabolism. However, the development of advanced analytical techniques, allowed for a more accurate assessment of dhCer's biological functions. It was later discovered that treatments with certain anticancer agents, such as fenretinide, led to an accumulation of dhCer due to the inhibition of dihydroceramide desaturase 1 (Des1).[5] This inhibition not only altered sphingolipid profiles but also induced autophagy, suggesting a potential antitumor mechanism. These findings overturned the notion of dhCer as merely an inactive precursor, revealing its active role in modulating apoptosis and autophagy. Given its influence on cellular metabolism, dhCer has been implicated in various diseases, including cancer, diabetes, and neurodegenerative disorders. Consequently, the dhCer/Cer ratio has emerged as a critical regulatory factor, especially considering that Cer can be further metabolized into sphingosine-1-phosphate (S1P), lipid that promotes tumor cell survival and proliferation. Current research thus focuses on modulating this ratio, with Des1 activity being a key target due to its central role in controlling the balance between dhCer and Cer.

### 1.4. Dihydroceramide desaturase 1 (Des 1):

The proposed mechanism for converting dihydroceramides into ceramides involves the participation of an enzyme-bound diiron-dioxo species at the active site, which initiates the reaction by abstracting the hydrogen atom at the C-4 position of the sphingoid base. This rate-limiting step is energetically demanding and is followed by a rapid abstraction of the C-5 hydrogen, resulting in the formation of a *trans* double bond between C-4 and C-5. Although the precise structure of Des1 and its active site remains incompletely resolved, progress has been made in identifying and designing active-site-directed inhibitors. These inhibitors are valuable tools for studying Des1 function and for exploring therapeutic strategies aimed at modulating the dhCer/Cer ratio in disease contexts.

### 1.5. Des1 inhibitors:

Many anticancer therapies leverage the inhibition of Des1 (dihydroceramide desaturase 1) as a key mechanism. The majority of Des1 inhibitors developed to date are sphingolipid analogs, designed to mimic the structure of dhCer while exhibiting higher affinity for the enzyme, thereby competitively inhibiting its natural substrate.

These sphingolipid analogues typically share key structural features that are critical for effective inhibition:

[5] Zheng, W.; Kollmeyer, J.; Symolon, H.; Momin, A.; Munter, E.; Wang, E.; Kelly, S.; Allegood, J. C.; Liu, Y.; Peng, Q.; Ramaraju, H.; Sullards, M. C.; Cabot, M.; Merrill, A. H. *Biochim. Biophys. Acta* **2006**, *1758*, 1864-1884.

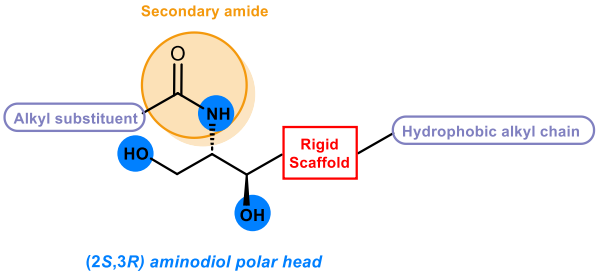


***Figure 2:*** *Key structural features of sphingolipid analogues Des1 inhibitors.*

GT11 was the first such analogue developed, incorporating a cyclopropene moiety at the position corresponding to the natural double bond in ceramide (Figure 3).[6] This design was inspired by the known inhibitory effects of cyclopropene fatty acids on other desaturase enzymes. Structure–activity relationship studies on GT11 revealed that certain features significantly enhance Des1 inhibition: specifically, the *anti*-2*S*,3*R* stereochemistry, the presence of a hydroxyl group at the C-1 position, and a secondary amide linkage.

Another potent Des1 inhibitor, XM462 (Figure 3), was later synthesized with a sulfur atom replacing the C-5 carbon. Further investigations into *N*-acyl chain modifications demonstrated that analogues containing ceramide-like alkyl chains in the secondary amide position exhibited the highest inhibitory activity among various tested substituents.[7]

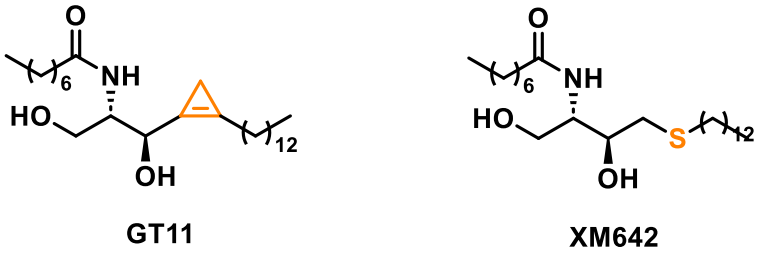


***Figure 3:*** *GT11 and XM642 Des1 inhibitors.*

### 1.6. Previous research conducted by SINTCARB research group:[8]

Previous efforts aimed at synthesizing more potent Des1 inhibitors, which directly precede the work presented in this study, were carried out by Pablo Rivero as part of his doctoral research in the group SINTCARB at the URV. His work focused on designing ceramide analogues incorporating rigid structural motifs in place of the natural double bond, with the goal of enhancing inhibitory activity through additional interactions in the active site of the enzyme.

#### 1.6.1. Prediction of 3D structure and active site of Des1 using AlphaFold2

To obtain a more accurate approximation of the Des1 active site—crucial for the rational design of potent inhibitors in the absence of an experimentally resolved crystal structure—the AlphaFold2 software was employed. AlphaFold2 is an artificial intelligence (AI) system developed by DeepMind that can predict three-dimensional (3D) structures of proteins from amino acid sequences with atomic level accuracy. The objective was to gain detailed structural insight into the enzyme's active site, enabling the identification of key molecular

[6] Triola, G.; Fabriàs, G.; Llebaria, A. *Angew. Chem.* **2001**, *113*, 2014–2016

[7] Muñoz-Olaya, J. M.; Matabosch, X.; Bedia, C.; Egido-Gabas, M.; Casas, J.; Llebaria, A.; Delgado, A.; Fabriàs, G. *ChemMedChem* **2008**, *3*, 946-953.

[8] Rivero, P. *Targeting Des1: Syntheses of Ceramide Analogues with a Rigid Scaffold, Inhibitory Assays, and AF2-Assisted Structural Insights Reveal PR280 as a Potent Inhibitor*. PhD thesis, Universitat Rovira i Virgili, **2024.**

interactions involved in Des1 inhibition and facilitating the targeted design of novel inhibitors.

AlphaFold2 evaluates the reliability of its predictions using the **predicted Local Distance Difference Test** (pLDDT) score, which ranges from 0 to 100. A pLDDT score above 90 indicates high confidence in the predicted structure, while regions scoring below 50 are considered unreliable and typically excluded from further analysis.

The predicted 3D structure of Des1 generated by AlphaFold2 (Figure 4) displayed a high level of confidence, with nearly the entire enzyme structure receiving pLDDT scores above 90, indicating strong reliability in the predicted folding and spatial arrangement.

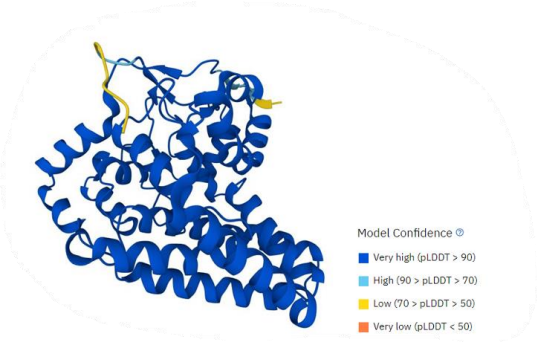


***Figure 4:*** *Predicted 3D structure of Des1 using Alphafold2.*

To achieve a more accurate representation of the enzyme's active site—given that AlphaFold2 predictions are based solely on the primary amino acid sequence—the catalytically essential non-heme oxo-diiron ($Fe_2O_2$) cofactor was manually incorporated into the model. With this addition, the first complete 3D model of Des1 containing the $Fe_2O_2$ active site was constructed (Figure 5).

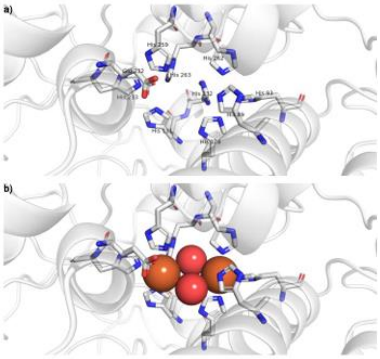


***Figure 5:*** *Predicted 3D structure of Des1 active site including the $Fe_2O_2$ cofactor.*

The active site of Des1 is characterized as a long and narrow cavity predominantly composed of apolar amino acids, as expected for a trans-membrane protein. However, the end of the cavity is enriched with polar residues—nine histidines and one glutamic acid—which supports the hypothesis that the catalytic cofactor is located in this region, stabilized through coordination with the donor groups from these polar residues, facilitating its proper positioning and function within the active site. Thus, the $Fe_2O_2$ cluster was places in such a way that one iron atom is coordinated by five histidine residues, while the second iron atom is coordinated by four histidines and one glutamic acid. This coordination geometry supports the proposed catalytic mechanism and provides a structural basis for rational inhibitor design.

The latest iteration of the artificial intelligence model, **AlphaFold 3**, released in 2024, enables the prediction of not only protein three-dimensional structures but also their interactions with a range of biomolecules—including DNA, RNA, ligands, and antibodies—with remarkable accuracy. Notably, this new model validated the positioning of the **$Fe_2O_2$** group previously proposed by our research group in collaboration with Prof. Xavier Barril (University of Barcelona).

### 1.6.2. Molecular docking studies with the Des1-$Fe_2O_2$ 3D predicted model

Molecular docking studies were previously conducted using the potent reference inhibitors GT11 and XM462, as well as the natural substrate dihydroceramide (dhCer), with the aim of elucidating key ligand-enzyme interactions involved in Des1 inhibition. These computational analyses revealed that the primary structural features contributing to the inhibitory activity of sphingolipid analogues against Des1 include:

- The spatial proximity of positions 4 or 5—where the rigid molecular scaffold is typically located—to the $Fe_2O_2$ cofactor complex.
- A folded conformation of the hydrophobic alkyl chains upon binding within the enzyme's active site.
- Formation of a hydrogen bond between the 3-hydroxyl group and one of the oxygen atoms of the $Fe_2O_2$ complex.
- Establishment of a hydrogen bond between the 1-hydroxyl group and either a histidine or glutamic acid residue within the active site of the enzyme.

### 1.6.3. Synthesis and Des1 inhibition activity of cyclopropenone's ceramide analogues

Based on the insights obtained from the aforementioned docking studies, a novel and more potent Des1 inhibitor was rationally designed, **PR280.** Specifically, a ceramide analogue incorporating a cyclopropenone moiety as a rigid scaffold was hypothesized to exhibit high inhibitory potency. The cyclopropenone group was expected not only to preserve the folded conformation of the hydrophobic alkyl chains upon binding to the Des1 active site, but also to engage in additional polar interactions with the $Fe_2O_2$ complex due to the presence of a carbonyl oxygen.

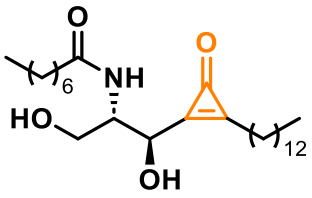


**PR280**

***Figure 6: PR280** ceramide analogue incorporating a cyclopropenone moiety.*

Following this revised understanding, a series of ceramide analogues containing cyclopropenone moieties were synthesized and evaluated for their Des1 inhibitory activity both in T98 intact cells and in T98 cell lysated.

Thus, cyclopropenone ceramide analogue **PR280** exhibited 86% inhibition of Des1 at a concentration of 10 μM in intact T98 cells, a level of activity comparable to that of XM462 (85% inhibition at 10 μM). Notably, **PR280** demonstrated enhanced potency in cell lysate assays, achieving 92% inhibition, surpassing the performance of XM462 (78% inhibition).

These results confirmed that compound **PR280** is a more potent Des1 inhibitor than both GT11 and XM462. Moreover, it exhibits a significantly lower $IC_{50}$ value (0.7 μM) compared to

GT11 ($IC_{50}$ < 20 μM) and XM462 ($IC_{50}$ = 8.2 μM), indicating a higher inhibitory efficiency at lower concentrations.

Subsequent biological investigations conducted in collaboration with Dr. Gemma Fabriàs (IQAC, CSIC, Barcelona), revealed that **PR280** treatment resulted in elevated levels of dihydroceramide (dhCer), a known consequence of Des1 inhibition. Interestingly, an unexpected increase in ceramide (Cer) levels was also observed (Figure 7):

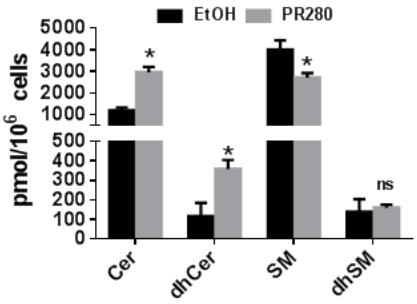


***Figure 7:*** *Variety of Cer and dhCer levels when PR280 inhibits Des1.*

This outcome is inconsistent with selective Des1 inhibition, as inhibition of the enzyme responsible for the conversion of dhCer to Cer should lead to decreased Cer levels. The observed increase in Cer therefore suggests that **PR280**, despite being a highly potent Des1 inhibitor, is not fully selective and give off-target effects, interacting with an additional unidentified enzyme that utilizes Cer as a substrate. As of the time of writing, this off-target activity remains uncharacterized and is currently under investigation in the frame of a collaboration with prof. Clarke at the Department of Medicine and Cancer Center of the Stonybrook University (New York).

### 1.6.4 Identification of ceramide analogues as potential Des1 inhibitors by virtual screening

Given that **PR280** demonstrated the highest inhibitory potency among the synthesized compounds, a **virtual screening** campaign was initiated with the objective of designing analogues with potentially enhanced Des1 inhibitory activity and improved selectivity to minimize off-target interactions. This virtual screening was conducted in collaboration with Prof. Xavier Barril (ICREA Research Professor, University of Barcelona) and focused on the systematic modification of the *N*-acyl chain at the amide substituent, while retaining the remainder of the **PR280** molecular scaffold unchanged.

The screening protocol included several rational design constraints. First, modifications were limited to commercially available carboxylic acids with truncated molecular weights to maintain drug-like properties. Additionally, preference was given to carboxylic acids containing quaternary carbon centers, as such structures are associated with increased binding selectivity and enhanced solubility and metabolic stability. In total, a virtual library of 2027 carboxylic acids were curated for potential amidation with the **PR280** backbone.

Subsequent molecular docking studies were conducted to evaluate the binding affinities of the resulting ceramide analogues. These simulations specifically assessed the preservation and optimization of key ligand-enzyme interactions previously associated with potent Des1 inhibition. From this dataset, the top 45 analogues were selected based on optimal docking scores and interaction profiles. Among these, 10 analogues were prioritized for synthesis, based on multiple criteria including the strength and number of predicted protein-ligand interactions, presence of additional stabilizing contacts, synthetic accessibility, and cost of the corresponding carboxylic acid precursors.

Each candidate compound was assigned a docking score reflecting the cumulative contribution of its predicted interactions with the Des1 active site. This scoring system enabled a comparative ranking of the analogues and guided the selection of the most promising candidates for experimental validation (Table 1):

***Table 1:*** *Ceramide analogues selected after the screening, docking, and considerations mentioned.*[8]

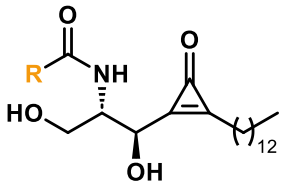


| Entry | R | Docking ranking [a] | Score [a] | Interactions with the active site of Des1 |
|---|---|---|---|---|
| **1** | 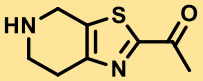 | 3 | -22.612 | - Parallel displaced π-stacking (Tyr170)<br>- H-bond: NH-carbonyl backbone |
| **2** | 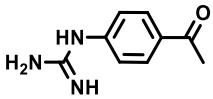 | 4 | -22.548 | - Parallel displaced π-stacking (Tyr170)<br>- H-bond: NH-carbonyl backbone |
| **3** | 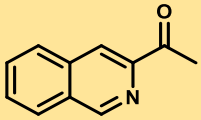 | 7 | -21.199 | - Parallel displaced π-stacking (Tyr170) |
| **4** | 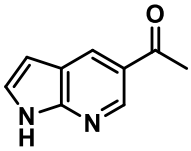 | 26 | -19.697 | - Parallel displaced π-stacking (Tyr170)<br>- H-bond: NH-carbonyl backbone |
| **5** | 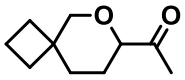 | 9 | -20.887 | - H-bond: OH-O (Tyr 120) |
| **6** | 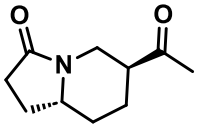 | 21 | -19.856 | - None |
| **7** | 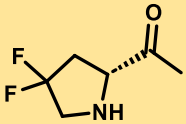 | 27 | -19.687 | -Weak H-bond: NH-π (Tyr170)<br>- *gem*-difluoro group in a non-polar environment. |
| **8** | 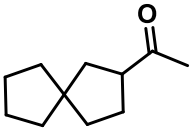 | 8 | -20.955 | - Aliphatic compound in a non-polar environment. |
| **9** | 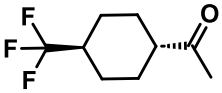 | 13 | -20.383 | - Aliphatic groups in a non-polar environment. |
| **10** | 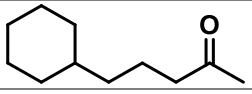 | 21 | -19.512 | - Aliphatic compound in a non polar environment. |

[a] Docking ranking and score resulted from docking studies against the predicted 3D structure model of Des1 by Alphafold 2 using virtual screening

## 2. Objectives

Based on the previous insights, the objective of the present study is to synthesize three **PR280** analogues incorporating basic functional groups on the *N*-acyl chain, selected from the top candidates identified through virtual screening and subsequent molecular docking calculations. These analogues were chosen based on their predicted inhibition activity and high selectivity as Des1 inhibitors.

The three selected analogues, designated **PR280-1**, **PR280-3**, and **PR280-7** (highlighted in orange in Table 1), were prioritized for synthesis and subsequent biological evaluation.

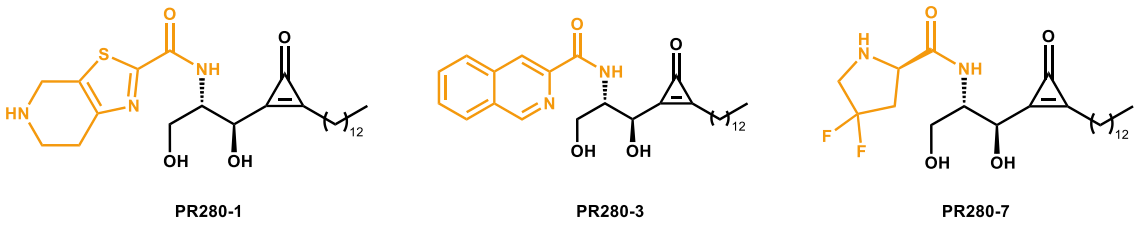


***Figure 8:*** *Three **PR280** selected analogues for synthesis and biological evaluation.*

**PR280-1,** incorporating a thiazole ring, is predicted to establish a hydrogen bond with a carbonyl group within the Des1 active site. Additionally, this analogue is expected to engage in parallel displaced π–π stacking interactions, potentially enhancing binding affinity.

**PR280-3** is also predicted to exhibit parallel displaced π–π stacking. Taking into account the aromatic nature of its *N*-acyl chain, its activity profile will provide insights into how planar, conjugated systems influence Des1 inhibition when positioned adjacent to the amide linkage.

**PR280-7**, although predicted to form a relatively weak hydrogen bond, contains a highly polar substituent ($CF_2$ motif). Its evaluation may help determine the influence of increased polarity within the Des1 active site. Furthermore, **PR280-7** is a non-planar analogue, making it a useful comparator to **PR280-1** and **PR280-3** in assessing the role of aromaticity and molecular planarity in inhibitory efficacy.

Although not explicitly confirmed by the docking experiments, the presence of basic functional groups might facilitate additional interactions that contribute to enhanced affinity for the enzyme.

The present work details the complete synthetic procedures used to obtain these three ceramide analogues. It includes the design and optimization of synthetic routes, as well as the full structural characterization of the newly synthesized compounds. **These studies aim to advance the development of potent and selective Des1 inhibitors with reduced off-target effects compared to the previous inhibitor synthetized PR280.**

## 3. Results and discussion

The target ceramide analogues were synthesized according to the synthetic pathway outlined in Scheme 3.

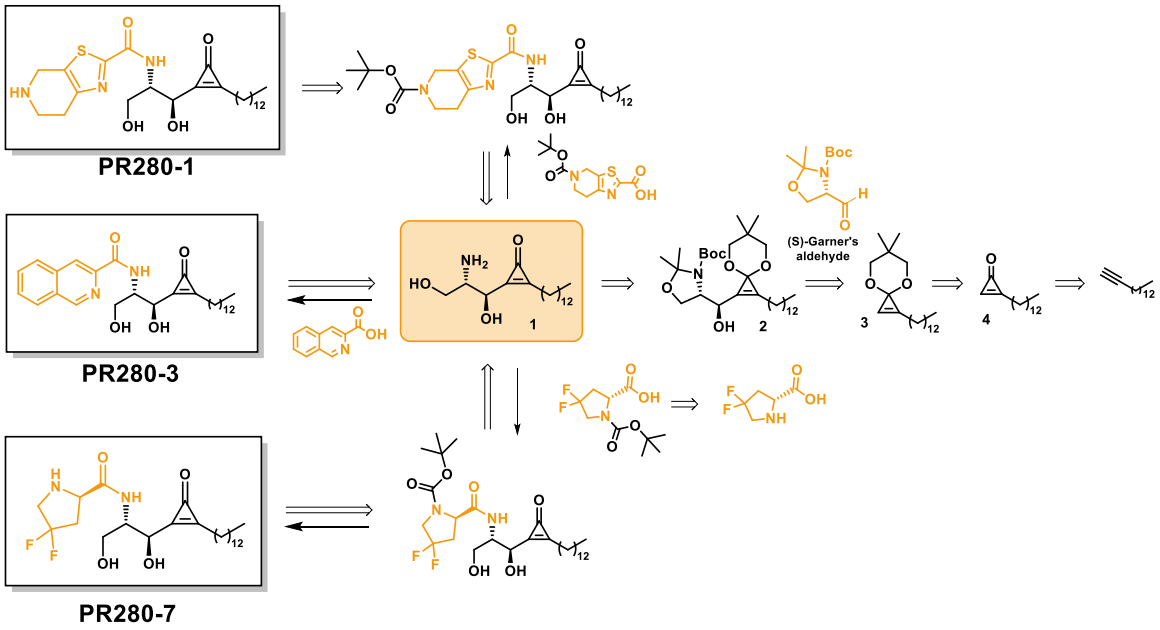


***Scheme 3:*** *General retrosynthetic scheme of the proposed ceramide analogues of this work.*

The three analogues—**PR280-1**, **PR280-3**, and **PR280-7**—were intended to be obtained via an amidation reaction between a common aminodiol **1** (Scheme 3) and the respective carboxylic acids, resulting in the formation of the corresponding ceramides.

The synthesis of this aminodiol intermediate had been already optimized in our group and performed by deprotection of the oxazolidine, Boc, and dioxaspiro acetal protecting groups presents in compound **2**. These protecting groups were introduced to avoid side reactions in the nucleophilic addition of the lithiated protected cyclopropenone derivative **3** to the (*S*)-Garner's aldehyde. 2-Trydecylcyclopop-2-en-1-one **4**, in turn was synthesized from 1-pentadecyne through a two-step process involving the formation of a difluorocyclopropene intermediate followed by hydrolysis.

### 3.2. Synthesis of target compounds

#### 3.2.1. Cyclopropenation reaction

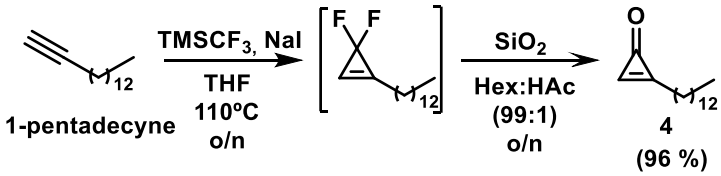


***Scheme 4:*** *General reaction of cyclopropenation from 1-pentadecyne.*

In the initial stage, 1-pentadecyne was treated with Ruppert–Prakash reagent ($TMSCF_3$)[9] in the presence of sodium iodide (NaI) at 110 °C to generate the difluorocyclopropene intermediate following the mechanisms depicted in Scheme 5

[9] Wang, F.; Luo, T.; Hu, J.; Wang, Y.; Krishnan, H. S.; Jog, P. V.; Ganesh, S. K.; Prakash, G. K. S.; Olah, G. A. *Angew. Chem.* **2011**, *123*, 7291–7295.

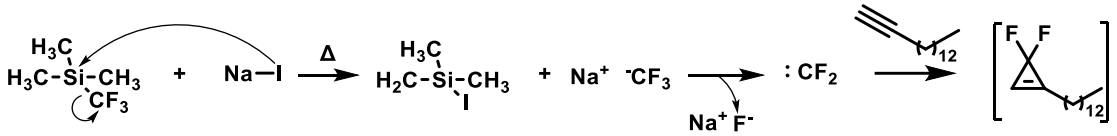

***Scheme 5:*** *Mechanism of formation of difluorocarbene and subsequent formation of difluorocyclopropene intermediate.*[10 11]

This transformation proceeds via *in situ* generation of difluorocarbene, which subsequently undergoes cycloaddition with the terminal alkyne to form the difluorocyclopropene intermediate (Scheme 5).

Difluorocyclopropene intermediate was submitted then to hydrolysis under mildly acidic conditions in a silica suspension, yielding the desired cyclopropenone **4** in **96 %** yield from **1-pentadecyne** (Scheme 4)**.**

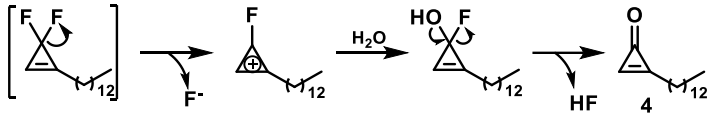

***Scheme 6:*** *Hydrolysis mechanism of difuorocyclopropene into the desired cyclopropenone 1.*[12]

### 3.2.2. Protection of cyclopropenone 4 into a dioxaspiro acetal

In order to perform the subsequent stereoselective nucleophilic addition to (*S*)-Garner's aldehyde, it was necessary to protect the cyclopropenone moiety. This protection prevents undesired side reactions due to the cyclopropenone's ambiphilic (both nucleophilic and electrophilic) nature.

The cyclopropenone was protected as a dioxaspiro acetal via reaction with neopentyl glycol under specific conditions (Scheme 7). Although cyclopropenone is relatively stable due to its aromatic character, direct acetalization typically requires harsh conditions, which often results in undesired side products such as geminal diols or hemiacetals.[13]

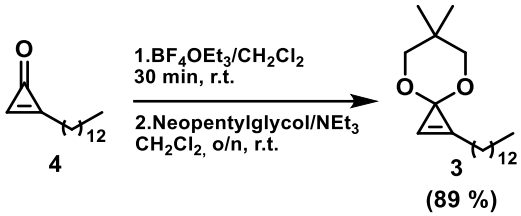

***Scheme 7:*** *Reaction of cyclopropenone acetalization*.

To circumvent this limitation, the cyclopropenone was first converted into a cyclopropenium ion by treatment with triethyloxonium tetrafluoroborate as a strong alkylating agent. This transformation yields a true 2π-aromatic species, enhancing stability.[14] Subsequent reaction of the cyclopropenium ion with neopentyl glycol under basic conditions—conditions now tolerated due to the increased stability conferred by aromaticity—afforded the desired dioxaspiro acetal **3** (Scheme 8).

[10] Wang, J.; Luis, J.; Pozo, C.; Sorochinsky, A. E.; Fustero, S.; Soloshonok, V. A.; Liu, H. *Chem. Rev*. **2014**, *114*, 2432–2506.

[11] Rullière, P.; Cyr, P.; Charette, A. B. *Org Lett* **2016**, *18*, 1988–1991.

[12] Cheng, Z. L.; Chen, Q. Y. Chin. *J. Chem*. **2006***, 24*, 1219-1224.

[13] Isaka, M.; Ejiri, S.; Nakamura, E. *Tetrahedron* **1992**, *48*, 2045- 2057.

[14] Yoshida, H.; Kinoshita, H.; Kato, T.; Kanehira, N.; Ogata, T.; Matsumoto, K. *Synthesis* **1987**, 393 394.

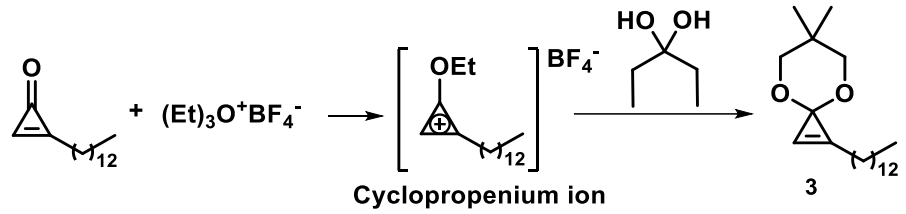


***Scheme 8:*** *Formation of protected derivative **3** via cyclopropenium ion.*

### 3.2.3. Diastereoselective addition of protected cyclopropenone to (*S*)-Garner's aldehyde

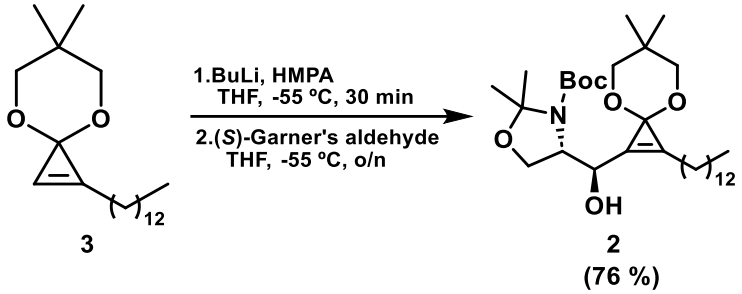


***Scheme 9:*** *General reaction of addition to the (S)-Garner's aldehyde.*

Garner's aldehyde (*tert*-butyl 4-formyl-2,2-dimethyloxazolidine-3-carboxylate) is a chiral and versatile reagent widely employed in the asymmetric synthesis of nitrogen-containing compounds.[15] In the context of this study, it plays a critical role by enabling the synthesis of the 2-amino-1,3-diol motif with the *anti*-stereochemistry required in the target ceramide analogues.[16]

The nucleophilic addition of the lithiated cyclopropenone derivative **3** to (*S*)-Garner's aldehyde proceeds with high diastereoselectivity under substrate control (Scheme 9). This selectivity arises from the ability to govern the stereofacial approach of the nucleophile to the chiral aldehyde. Depending on the reaction conditions—specifically whether the system operates under chelation or acyclic (Felkin-Anh) control—the stereochemical outcome can be directed toward the *syn* or the *anti*-diastereomer. Both diastereomers can be obtained with high levels of stereoselectivity, highlighting the utility of this transformations in stereocontrolled synthesis.

*Syn-selectivity (Cram's Chelation model)*[17]

In the presence of a chelating counterion—typically a metal cation such as $Li^+$, $Mg^{2+}$, $Zn^{2+}$—nucleophilic addition to α-chiral aldehydes proceeds under **chelation control**. The metal ion can simultaneously coordinate with the carbonyl oxygen and a neighboring Lewis-basic substituent (e.g. an alkoxy or amino group) on the α-carbon, forming a chelate ring. This bidentated coordination determines the reactive conformation on the transition state, thereby restricting the approach of the nucleophile—following the so-called Burgi Dunitz trajectory (107 °)—to a specific face of the carbonyl substituent. This enforced geometry leads to high diastereoselectivity, typically favoring the *syn* or *anti* diastereomer depending on the nature of the nucleophile and the metal ion involved.

[15] Garner, P. *Tetrahedron Lett*. **1984**, *25*, 5855–5858.
[16] Passiniemi, M.; Koskinen, A. M. P. *Beilstein J. Org. Chem*. **2013**, *9*, 2641–2659.
[17] Cram, D. J.; Abd Elhafez, F. A. J. *Am. Chem. Soc*. **1952**, *74*, 5828-5835.

The chelating counterion thus plays a **critical role in directing stereochemical outcome** by stabilizing a specific transition state geometry, overriding steric or electronic preferences that would dominate under non-chelating (acyclic) conditions.

In the reaction under study, chelation occurs between $Li^+$, the metal counterion of the nucleophilic reagent BuLi, the carbonyl oxygen of the aldehyde, and the carbonyl oxygen of the Boc protecting group, forming a seven-membered chelate ring (Scheme 10). This chelate imposes a well-defined transition state geometry—directing the nucleophile to approach from the more accessible face of the carbonyl. This face corresponds to the side bearing the smallest substituent on the α-carbon—typically the hydrogen atom—thereby minimizing steric interactions. As a result, nucleophilic attack preferentially occurs on the Si face of the carbonyl, leading predominantly to the syn diastereomer.

*Anti*-selectivity (Felkin-Anh model):

In the absence of chelating counterions, the reaction proceeds via the acyclic (Felkin–Anh) control (Scheme 10).[18] in this model, the largest substituent on the α-carbon (in this case, the Boc-protected nitrogen) adopts an orthogonal orientation to the carbonyl group, thereby reducing unfavorable interactions with the incoming nucleophile. The smallest substituent on the α-carbon is positioned adjacent to the carbonyl substituent—specifically, near the aldehyde hydrogen—to reduce steric hindrance during nucleophilic attack along the Bürgi-Dunitz trajectory.

This stereoelectronic arrangement leads to the preferential formation of the *anti*-diastereomer, in contrast to the *syn* product typically observed under chelation control. The Felkin–Anh model is particularly applicable when chelation is disfavored—such as in the presence of non-chelating counterions, when the α-substituent lacks a Lewis-basic site, or when strongly coordinating additives (such as hexamethylphosphoramide (HMPA), [19] used here) solvate the metal cation and thereby prevent effective chelation. Additionally, as an aggregation-disrupting additive, HMPA, renders the cyclopropenone anion more nucleophilic.

[18] Cherest, M.; Felkin, H.; Prudent, N. *Tetrahedron Lett.* **1968**, *18*, 2199-2204.
[19] Herold, P. Helv. *Chim. Acta* **1988**, *71*, 354–362.

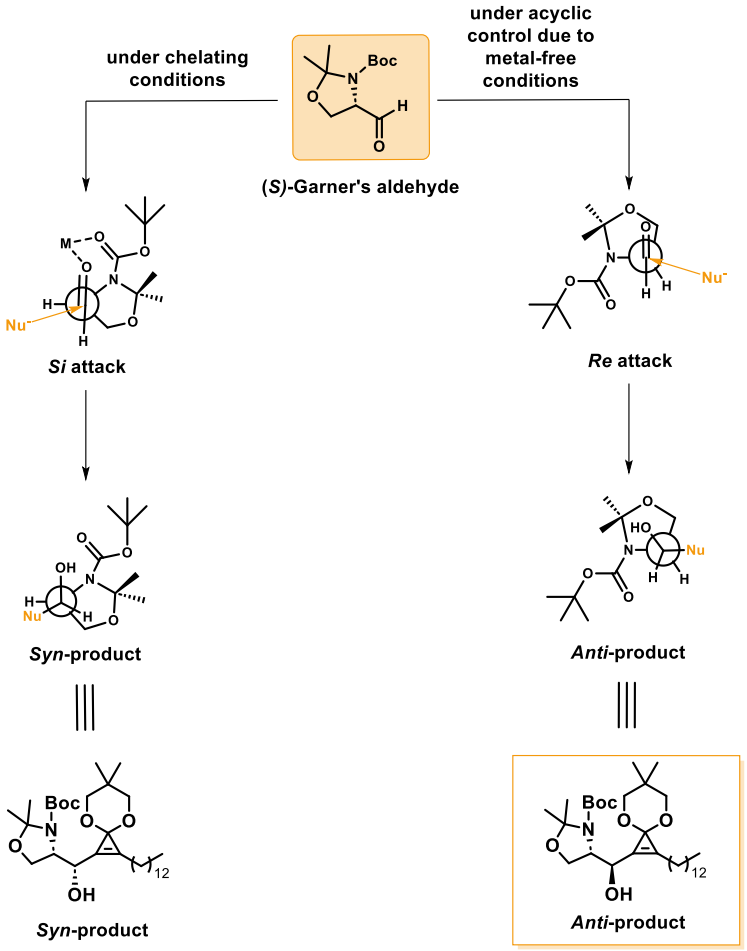


***Scheme 10:*** *Mechanisms of the two possible diastereoselective additions through Felkin-Anh and Cram's models.*

These stereoelectronic considerations are crucial in obtaining the correct configuration of the 2-amino-1,3-diol subunit in the synthesized ceramide analogues, as required for optimal Des1 inhibitory activity.

In this step, *n*-butyllithium was employed as the base to abstract the acidic proton from the cyclopropenone acetal **3** (Scheme 11).

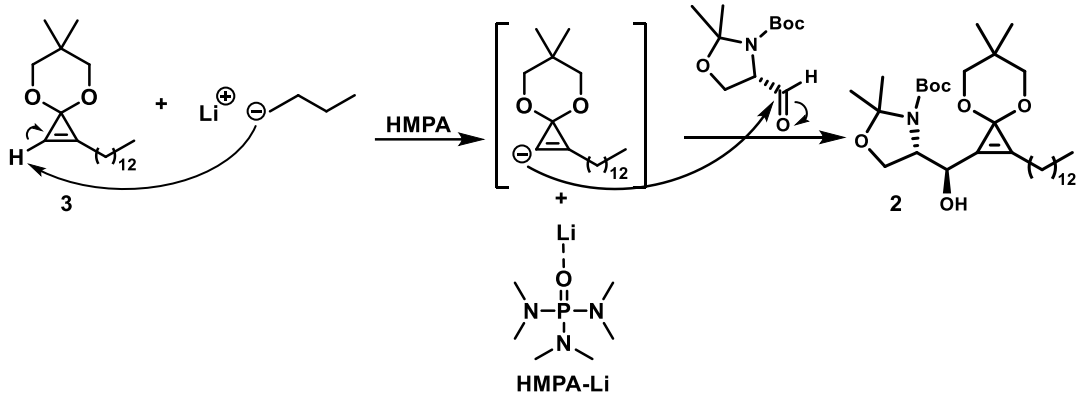


***Scheme 11:*** *Detailed process for the diastereoselective addition of protected cyclopropenone 3 to (S)-Garner's aldehyde.*

The choice of solvent also plays a crucial role. Tetrahydrofuran (THF) was used because it is a coordinating solvent capable of interacting with Lewis's acids such as lithium ions.[20] This coordination increases the electron density around lithium, diminishing its ability to act as a Lewis acid toward other Lewis bases such as the carbonyl group of Garner's aldehyde. As a result, lithium-carbonyl chelate formation is further suppressed.

These combined factors—HMPA as a lithium-sequestering agent, THF as a coordinating solvent, and low temperature—led to high *anti*-diastereoselectivity, with 97:3 *anti*:*syn* diastereomeric ratio, confirming the successful stereocontrol of the reaction.

To confirm the structure of the protected aminodiol **2**, a $^{1}$H NMR analysis was performed. As observed in previous studies,[8] the compound exhibited broad and poorly defined signals at room temperature. This behavior is attributed to the presence of **two rotameric conformers** probably due to the presence of the protecting Boc group, coexisting in solution, each giving rise to similar yet distinct sets of proton signals. These overlapping signals lead to broad or split peaks in the room-temperature spectrum.

To improve spectral resolution and obtain a more representative fingerprint, the $^{1}$H NMR experiment was repeated at 50 °C, where the rapid interconversion between the Boc-rotamers led to signal averaging. This temperature-dependent behavior is particularly evident in the signal at **2.47 ppm** (Figure 10), corresponding to the methylene protons on C-6 on the alkyl chain, which is also adjacent to the alkenyl carbon of the protected cyclopropenone moiety.

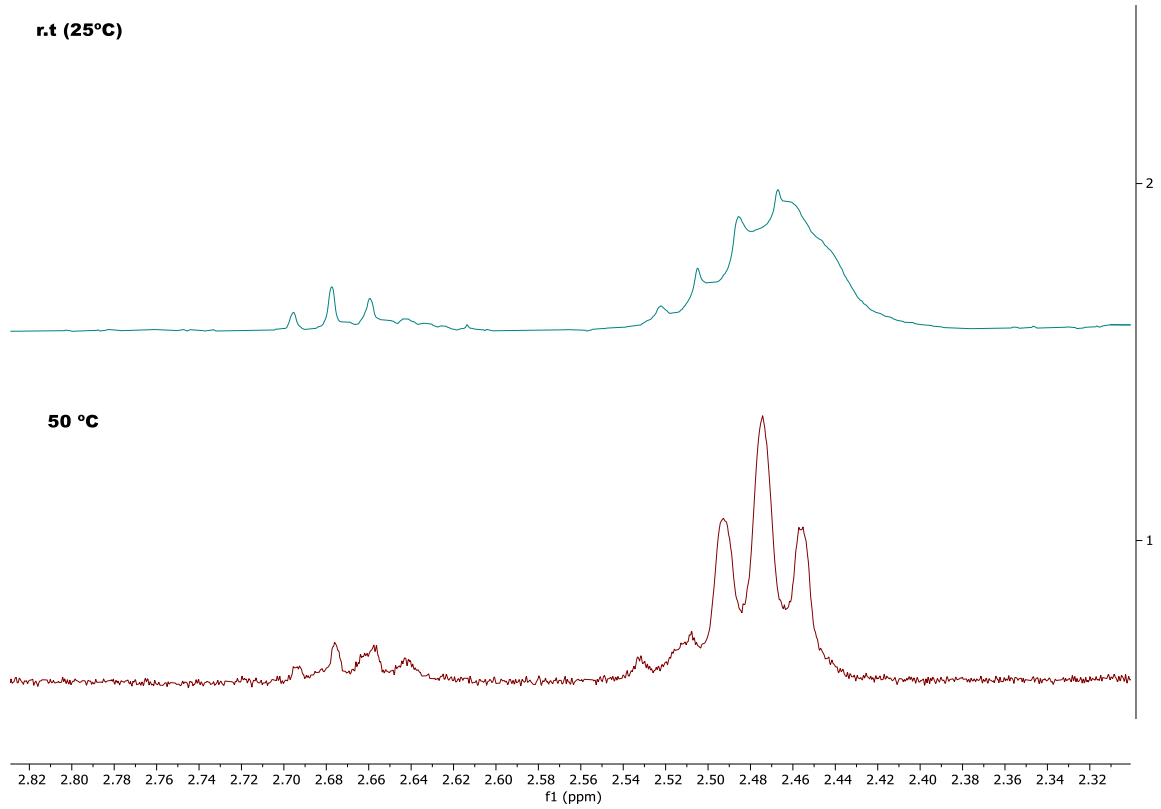


***Figure 9:*** *Effect of temperature in $^{1}$H NMR spectrometry H-3 signal of compound 3*.

[20] Williams, L.; Zhang, Z.; Shao, F.; Carroll, P. J.; Joullié, M. M. *Tetrahedron* **1995**, *52*, 11673–11694.

### 3.2.4. Deprotection of the oxazolidine, Boc and dioxaspiro acetal protecting groups

To obtain the aminodiol and cyclopropenone functional groups necessary for subsequent *N*-acylation steps and the synthesis of the final ceramide analogues, complete deprotection of compound **2** was required. This involved removing all three protecting groups: the mixed-*N*,*O*-acetal, the *tert*-butyl carbamate (Boc), and the neopentyl acetal. All these groups are acid-labile and can be removed under acidic conditions; therefore, a one-step, simultaneous acidic deprotection was performed (Scheme 12).

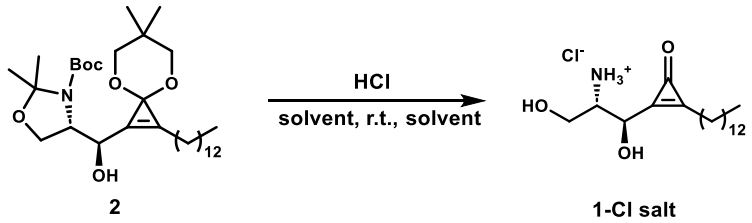


**2** **1-Cl salt**

***Scheme 12:*** *Reaction of deprotection of the protected aminodiol **2**.*

Hydrochloric acid (HCl) was selected as the deprotecting agent. This decision was based on prior observations in our group, where the use of trifluoroacetic acid (TFA) led to the formation of the corresponding trifluoroacetamide.[8] In contrast, the use of HCl enables the generation of the more manageable hydrochloride salt of the aminodiol **1**.

However, applying the original methodology using HCl resulted in low yields, prompting a series of optimization experiments to improve the efficiency of the deprotection step (Table 2).

***Table 2****: Optimization for the deprotection reaction of protected aminodiol **2**.*

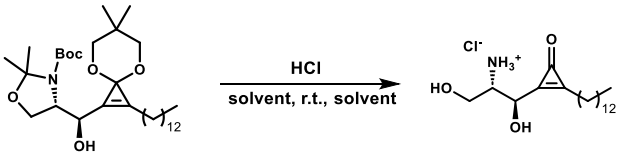


**2** **1-Cl salt**

| Entry | Solvent | Concentration (mmol/mL) | HCl | HCl (equiv.) | Time (h) | Yield (%) |
|---|---|---|---|---|---|---|
| **1**[8] | $H_2O$ | 0.04 | 2M in $Et_2O$ | 12 | 3 | 40 |
| **2** | 1,4-Dioxane | 0.02 | 1M in $H_2O$ | 30+50+16 | 24 | 70 [a] |
| **3** | 1,4-Dioxane | 0.04 | 4M in dioxane | 96 | 3 | >99 [a] |

[a] Yields determined by $^1$H-NMR spectroscopy using benzyl ether as an internal standard.

The initial experiment followed the original methodology employing 12 equiv. of HCl in diethyl ether, under biphasic conditions (Table 2, entry 1). After 3 hours, moderate yield of 40 % was observed by NMR analysis, and extending the reaction time beyond did not improve the yield.

Subsequently, the HCl amount was increased to 30 equivalents, and the solvent was changed from water to 1,4-dioxane to promote a more homogeneous reaction medium (Table 2, entry 2). After 3 hours, thin-layer chromatography (TLC) still indicated the presence of unreacted starting material. Additional portions of HCl—50 and 16 equivalents

respectively— were added over a further 10 hours, bringing the total to 86 equivalents, yet incomplete conversion was still observed. Increasing the HCl to 96 equivalents and extending the reaction time to 24 hours resulted in complete consumption of the starting material, affording the aminodiol product in 70 % yield (Table 2, entry 2).

Building on these findings, a third reaction assay was designed to maximize efficiency by introducing 96 equivalents of HCl from the outset (Table 2, entry 3). Additionally, dioxane was used as the solvent for the HCl solution, enhacing both the homogeneity and acidity of the reaction medium.
This optimized setup resulted in **quantitative conversion (>99 %)** within just **3 hours**, representing a significant improvement over previous conditions.

Consequently, the optimized protocol in was adopted for the deprotection step.

### 3.2.5. Neutralization of aminodiol hydrochloride salt (1-Cl salt)

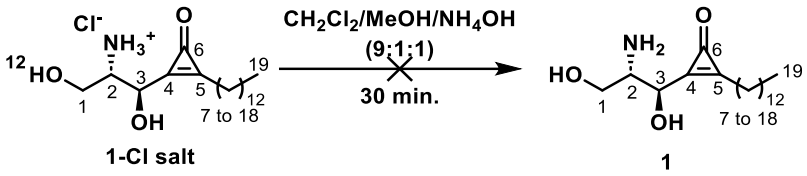


***Scheme 13:*** *Neutralization procedure of 1-Cl salt.*

Prior to the *N*-acylation reactions, the aminodiol hydrochloride salt (**1-Cl salt**) was first subjected to neutralization by stirring it with a ternary solvent mixture of $CH_2Cl_2$/MeOH/$NH_4OH$ (Scheme 13). However, neutralization did not proceed, and the free aminodiol **1** could not be obtained.

No conversion was observed during the attempted neutralization, as confirmed by $^1$H NMR spectroscopy. Reaction samples taken at various time intervals consistently showed a proton signal at **δ = 3.64 ppm**, corresponding to **H-2**, the proton on the carbon adjacent to the amine (Figure 11). This chemical shift matches that reported for the hydrochloride salt form **1-Cl salt**, according to prior studies in our grup. In contrast, the signal for H-2 in the neutral form of aminodiol **1** is expected to appear highfield (**δ = 3.09 ppm**), which was never observed under these conditions. Thus, the neutralization was completely unsuccessful, and the compound remained exclusively in its protonated salt form.

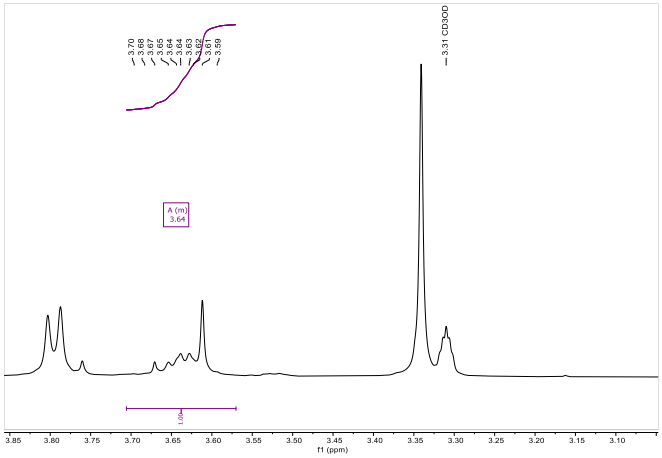


***Figure 10:*** *H-2 signal of **1-Cl salt** was the only one observed in $^1$H NMR spectroscopy.*

To isolate the free base, a flash column chromatography was performed on silica gel using a $CH_2Cl_2$/MeOH (96:4) mobile phase doped with 0.2% $NH_4OH$. Analysis of the purified fractions by $^1H$ NMR confirmed the appearance of the H-2 signal at δ = 3.09 ppm, indicating successful neutralization during chromatography rather than during the prior neutralization attempt.

However, the neutralized aminodiol **1** proved to be highly unstable. Even when stored under inert atmosphere at low temperature, it decomposed within 24 hours into a complex mixture of degradation products. Among these, one was identified and characterized as the enamine derivative resulting from dehydration of **1** (Scheme 14).

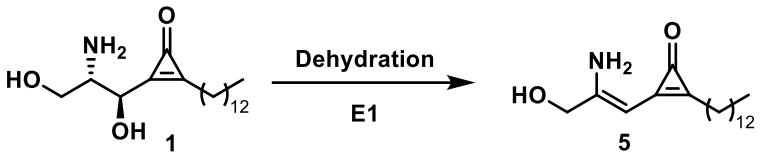


***Scheme 14:*** *Dehydration of **1** leading to the enamine **5**.*

This elimination product was confirmed through high-resolution mass spectrometry (**HRMS, ESI$^+$**) and $^1H$ NMR spectroscopy. The other degradation products could not be fully identified due to the complexity of the resulting mixture, which likely includes species formed via self-condensation, amine-cyclopropenone addition reactions, polymerizations, or further eliminations. A complete isolation and characterization of these decomposition products was beyond the scope of this study.

Given the poor stability of the neutralized aminodiol **1** and the need for additional purification to obtain it, subsequent *N*-acylation reactions were carried out directly using the crude hydrochloride **1-Cl salt**, without neutralization or further purification.

Importantly, compound **1-Cl salt** demonstrated excellent stability. Monitoring by $^1H$ NMR over several weeks and under moderate to high temperatures revealed no signs of decomposition, in contrast to its neutral counterpart. This stability, along with the synthetic practicality of avoiding further purification, justified the use of **1-Cl salt** directly in the final stages of the synthesis.

### 3.2.6. 5th step: Optimization of the *N*-acylation reaction conditions

Direct amidation between a carboxylic acid and an amine is generally inefficient under mild conditions due to the competing acid–base reaction that leads to the formation of a non-reactive ammonium carboxylate salt. At room temperature, this salt is thermodynamically favored and significantly reduces the nucleophilicity of the amine and the electrophilicity of the acid, effectively halting amide bond formation. To overcome this, harsh thermal conditions are often required, which not only limit functional group compatibility but also pose a substantial risk of racemization, particularly at stereogenic centers adjacent to the carboxylic acid.

In contrast, peptide-coupling strategies employing activating agents—such as carbodiimides (e.g., DCC, EDC), uronium salts (e.g., HBTU, HATU), and phosphonium reagents (e.g., PyBOP, BOP)—offer a significantly more efficient and versatile approach to amide bond formation. These methods function by converting the carboxylic acid into a highly reactive intermediate that readily undergoes nucleophilic attack by the amine under mild, typically room-temperature conditions. This approach effectively circumvents the formation of unreactive ammonium carboxylate salts, which predominate in direct acid–amine mixtures, and crucially reduces the risk of racemization that often accompanies

high-temperature amidation. As such, peptide-coupling reagents have become essential tools in modern synthetic chemistry, particularly for the construction of structurally complex or stereochemically sensitive amides and peptides.

The *N*-acylation of **1-Cl salt** was then conducted using a **HATU/DIPEA-mediated amide coupling** methodology, given the poor stability for the free amine (Scheme 15).[21] Actually, the hydrochloride salts of amine reactants are often used for *N*-amidation reactions with carboxylic acids or their derivatives, as they are typically more stable, easier to handle, and often commercially available, with *in situ* neutralization allowing for efficient coupling under mild conditions.

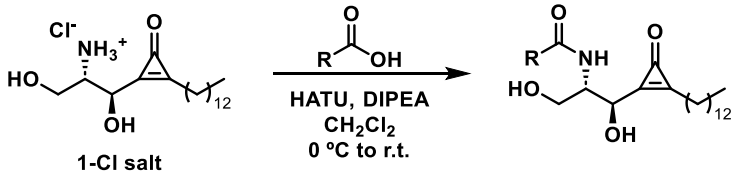


***Scheme 15:*** *General conditions for the N-acylation reactions performed.*

The use of HATU (O-(7-azabenzotriazol-1-yl)-*N,N,N',N'*-tetramethyluronium hexafluorophosphate) in combination with DIPEA (*N,N*-diisopropylethylamine) represents a widely adopted and highly efficient strategy for amide bond formation, particularly in peptide synthesis. This method relies on the *in-situ* activation of carboxylic acids to form reactive uronium intermediates, which then couple with amines under mild conditions to yield the corresponding amides.
The reaction proceeds according to the mechanism depicted in Scheme 16.
Thus, the carboxylic acid is first activated by HATU in the presence of DIPEA, forming a reactive OAt (7-azabenzotriazole) ester intermediate. The amine nucleophile then attacks this activated species, resulting in the formation of an amide bond. The presence of DIPEA not only facilitates activation by deprotonating the carboxylic acid and the amine, but also scavenges the generated acids, maintaining a neutral-to-basic environment conducive to coupling. When using hydrochloride salts, additional excess of DIPEA is used to neutralize the salt.
The advantages of this method over other coupling protocols are:

- High efficiency and yields: HATU-mediated couplings typically proceed rapidly and cleanly, even with hindered or poorly reactive substrates.
- Low racemization risk: The use of OAt esters significantly reduces epimerization at stereocenters, making this method ideal for peptide synthesis.
- Broad substrate scope: Effective for a wide range of carboxylic acids and amines, including secondary and aromatic amines.
- Mild reaction conditions: Reactions are usually performed at room temperature in polar aprotic solvents (e.g., DMF, NMP), making the method compatible with base-sensitive functional groups.
- Operational simplicity: HATU and DIPEA are commercially available, easy to handle, and require no special precautions beyond standard dry conditions.
- Compared to carbodiimide-based couplings (e.g., DCC or EDC), HATU offers faster reaction rates, fewer side products (e.g., no urea by-products), better solubility and cleaner purification. When compared with other uronium or phosphonium reagents (e.g., HBTU, PyBOP), HATU generally provides higher reactivity and lower racemization, especially important in peptide and complex amide syntheses.

[21] Carpino, L. A.; El-Faham, A. *J. Org. Chem.* **1995**, *60*, 3561–3564.

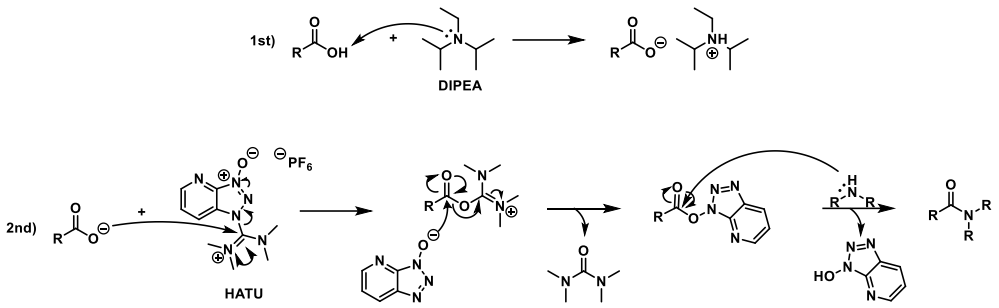


***Scheme 16:*** *General mechanism of HATU/DIPEA-mediated amide coupling amidation.*

To maximize the yield of the amidation step, two preliminary experiments were performed using different amounts of HATU and DIPEA (Table 3).

***Table 3****: Impact of HATU and DIPEA equivalents in reaction's performance.*

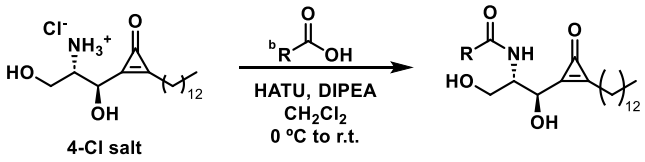


| Entry | HATU equivalents | DIPEA equivalents | Yield (%) |
|---|---|---|---|
| **1** | 1.1 | 1.1 | 11.3 [a] |
| **2** | 1.5 | 3.0 | 57 [a] |

[a] The yield of the amidation step was determined by estimating the amount of starting 4-Cl salt in the deprotection crude via $^1$H NMR spectroscopy using benzyl ether as the internal standard [b] The carboxylic acid used in both trials was the thiazole-containing acid, although the results were considered representative for all three acids employed in this study.

In both experiments, the carboxylic acid was used at 1.1 equivalents, and **1-Cl salt** (1.0 equiv.) was the limiting reagent.

In the first experiment, standard equivalents of HATU and DIPEA were used. This resulted in low yields of the desired product. Subsequently, the second experiment employed increased equivalents of both HATU and DIPEA, with a DIPEA:HATU ratio of 2:1. This adjustment was based on literature precedents indicating that using double the excess of base (or even more) relative to the coupling reagent is generally beneficial for amide bond formation.[22]

This optimized ratio of 1.5 equivalents of HATU and 3.0 equivalents of DIPEA was used in all subsequent amidation reactions.

[22] a) Guarrochena, X.; Kanellopoulos, P.; Stingeder, A.; Rečnik, L.-M.; Feiner, I. V. J.; Brandt, M.; Kandioller, W.; Maina, T.; Nock, B. A.; Mindt, T. L.. *Pharmaceutics* **2024**, *16*, 392. b) Bellavita, R.; Braccia, S.; Piccolo, M.; Białecki, P.; Ferraro, M. G.; Graziano, S. F.; Esposito, E.; Donadio, F.; Galdiero, S. *Int. J. Biol. Macromol*. **2025**, *292*, 139219.

### 3.2.7. Final stage amidation for the synthesis of Ceramide Analogue PR280-3

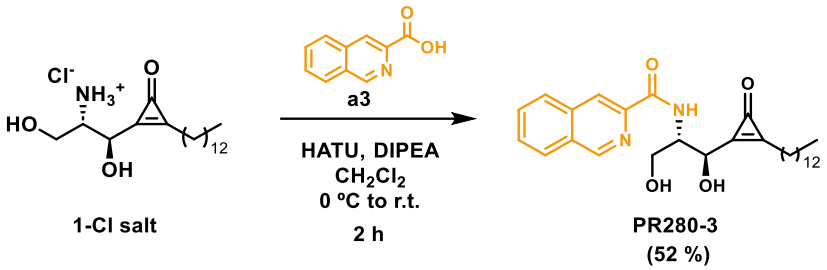


***Scheme 17:*** *Reaction of synthesis of* ***PR280-3****.*

Using the optimized conditions, carboxylic acid **a3** was subjected to amidation reaction (Scheme 17). The reaction progress was monitored by TLC, with disappearance of starting material and appearance of a less polar spot corresponding to the product. This shift in polarity reflects the loss of hydrogen-bonding capability when the amine is converted to an amide.

For compound **PR280-3**, the isolated yield of the amidation step was **52 %**, based on the estimation of the amount of starting material from the crude of the preceding deprotection step.

### 3.2.8.- Final stage amidation for the synthesis of Ceramide Analogue PR280-7

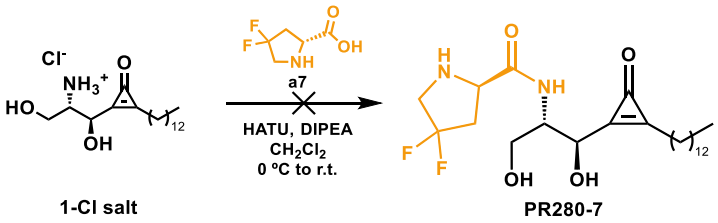


***Scheme 18:*** *First* ***PR280-7*** *synthesis reaction attempt.*

An initial amidation reaction to obtain **PR280-7** was performed with **a7** as the acylating agent and the aminodiol hydrochloride salt (**1-Cl salt**) as the nucleophile (Scheme 18). The reaction was monitored by TLC, and after 20 hours, some starting material was still present. After 21 hours, a sample analyzed by $^{1}$H NMR no longer showed signals of the starting material, and the reaction was stopped.

Purification by flash column chromatography allowed isolation of some apolar fractions, none of which matched the desired product.

The failure was likely attributable to the use of an amino acid–based acylating agent, which exists predominantly as a zwitterion and therefore exhibits limited solubility under the reaction conditions. This issue was further compounded by the insufficient excess of DIPEA employed in the initial, unoptimized amidation protocol (conditions of Table 3, entry 1). Furthermore, the absence of protection on the pyrrolidine nitrogen may have facilitated undesidered homoacylation at this site, competing with the intended coupling on the amine **1-Cl salt**.

Additionally, the enamine product **5** from elimination of the aminodiol was detected in the crude, confirming partial decomposition during the reaction.

To circumvent the lack of reactivity, the nitrogen of the difluorinated amino acid was protected as a *tert*-butyl carbamate (Scheme 19):[23]

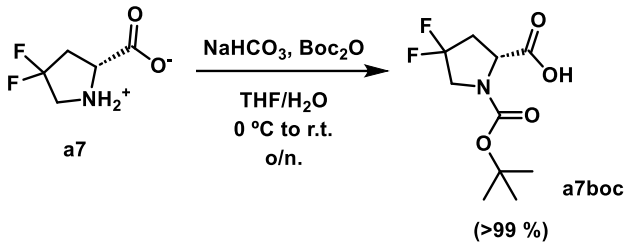


***Scheme 19**: Boc protection of the amino acid nitrogen.*

$NaHCO_3$ (1.5 equiv.) and $Boc_2O$ (1.1 equiv.) were used to perform the protection reaction. The crude product was purified by flash column chromatography, yielding the *N*-Boc-protected acid in quantitative yield (>99 %).

The amidation was assayed using the *N*-Boc-protected difluoro proline acid, and **1-Cl salt** under the optimized conditions (Scheme 20).

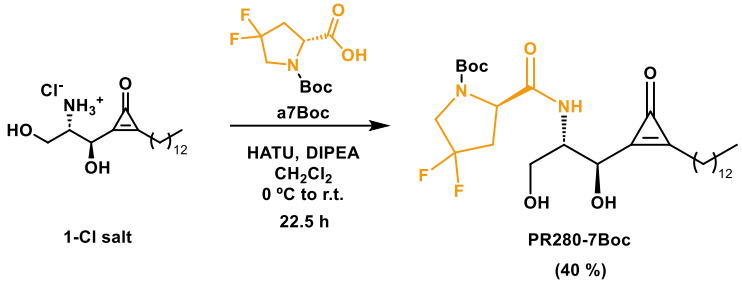


***Scheme 20**: Amidation reaction using N-Boc-protected amino acid **a7boc**.*

TLC indicated complete consumption of starting material after **22.5 h**, with a single apolar spot matching the expected product. Product was isolated by flash chromatography, yielding **PR280-7Boc** with an isolated yield of **40 %**.

Boc deprotection was carried out under acidic conditions using HCl (12.3 equiv.) in dioxane (Scheme 21).[24]

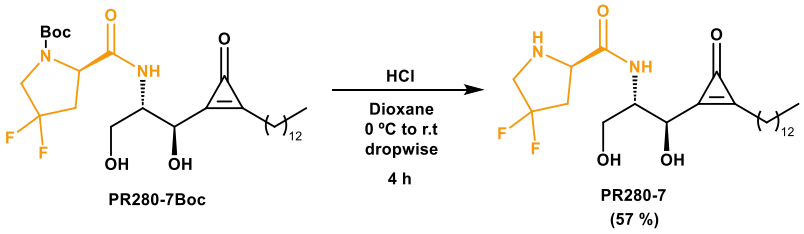


***Scheme 21**: Boc deprotection to yield **PR280-7**.*

TLC showed disappearance of starting material and appearance of a more polar spot consistent with the free pyrrolidine moiety. Reaction was complete after **4 h**. The ceramide product was isolated via flash chromatography with a **57 %** yield for this step.

[23] Yadav, G. D.; Singh, S. *RSC Adv* **2016**, *6*, 100459–100466.
[24] Cohen, M.; Bretler, U.; Albeck, A. *Protein Sci.* **2013**, *22*, 788–799.

### 3.2.9. Final stage amidation for the synthesis of Ceramide Analogue PR280-1

In this case, the thiazole-containing amino acid was already available in its *N*-Boc-protected form, which was used directly in the amidation with **1-Cl salt**:

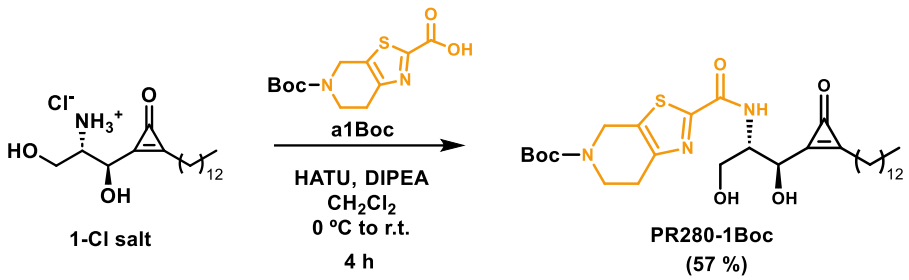


***Scheme 22:*** *Amidation to synthesize* ***PR280-1Boc.***

TLC showed complete reaction after **4 h**. A single apolar TLC spot consistent with the product was isolated. Product **PR280-1Boc** was obtained via flash column chromatography with an isolated yield of **57 %**, based on the estimation of the amount of starting material from the crude of the preceding deprotection step.

Subsequent Boc deprotection was performed with HCl (12.3 equiv.) in dioxane (Scheme 23).[24]

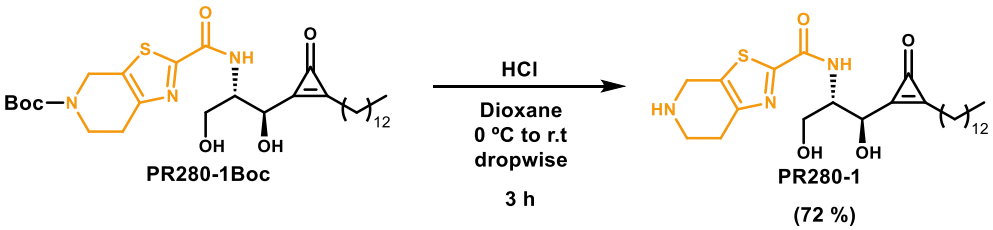


***Scheme 23:*** *Deprotection reaction to synthesize* ***PR280-1****.*

Reaction was complete in **3 h**, as judged by TLC. Flash column chromatography afforded pure **PR280-1** in **72 %** yield for this deprotection step.

### 3.3 Overall yields for each PR280 analogue synthetsized

Yields for the overall synthetic routes were 33 % for **PR280-3** (5 steps), 26 % for **PR280-1** (6 steps), and 13 % for **PR280-7** (7 steps).

### 3.4 Structural elucidation of the *N*-acylated products.

Obtaining of **PR280-1, PR280-3** and **PR280-7** was confirmed by $^{1}$H NMR, $^{13}$C NMR, COSY, HSQC spectroscopy and High-resolution mass spectrometry (HRMS).

Key NMR spectral features confirming successful amide formation included:

1- **Downfield shift of H-2** compared to its position in **1-Cl salt** and neutralized aminodiol **1**, due to **deshielding** from the amide group. HSQC and $^{13}$C NMR confirmed the correlation with a carbon adjacent to a nitrogen atom (55-56 ppm).
2- **H-3 proton signal** at 4.8–5.0 ppm, consistent with its attachment to a carbon bearing a hydroxyl group, corroborated by HSQC.
3- **Diastereotopic protons H-1 and H-1'** at 4-3.7 ppm confirmed via $^{13}$C NMR and HSQC.

Additionaly, HRMS confirmed the identity for the compound by providing an accurate mass of the expected molecular ion in an error lower that 3 ppm.

Full NMR and IR spectra, as well as optical rotation data $[\alpha]^{25}{}_{D}$ values for all synthesized compounds and their Boc-protected acid precursors (**PR280-7Boc** and **PR280-1Boc**), are provided in the **Annexes** and **Experimental Section**.

## 4. Experimental section

### General considerations

All reagents were purchased from Sigma Aldrich, Alfa Aesar or Carbosynth chemical companies. All solvents, HMPA and DIPEA were dried with activated 3Å-molecular sieves (MS) and were stored for 48 hours before being used to ensure dehydration and prevent any residual moisture from affecting the reaction outcome. 3Å MS were activated by heating under high vacuum at 260 °C for 10 h and then were stored at 165 °C. $^{1}$H and $^{13}$C spectra were recorded on a Varian® Mercury VX 400 or on a Bruker® Avance Ultrashield (400 MHz and 100.6 MHz respectively) spectrometer. NMR signals were fully assigned by COSY and HSQC. All chemical shifts are quoted on the δ scale in ppm using the residual solvent as internal standard ($^{1}$H NMR: $CDCl_3$ = 7.26; $^{13}$C NMR: $CDCl_3$ = 77.16; $^{1}$H NMR: MeOD = 3.31; $^{13}$C NMR: $CD_3OD$ = 49.0). Coupling constants (*J*) are reported in Hz with the following splitting abbreviations: s = singlet, d = doublet, t = triplet, q = quartet, p = pentuplet, sext = sextet, br s = broad singlet, br d = broad doublet, br t = broad triplet and br q = broad quartet, app = apparent. Infrared (IR) spectra were recorded on a JASCO FTIR-600 plus Fourier Transform Infrared Spectrophotometer wavenumbers (ṽ) in $cm^{-1}$. High resolution mass spectra were recorded on an Agilent® 1100 series LC/MSD instrument using electrospray ionization by the *Servei de Recursos Científics I Tècnics (URV)*. Optical rotations were measured on a Perkin–Elmer® 241 polarimeter with a path length of 1.0 dm and are reported with implied units of $10^{-1}$ deg $cm^2$ $g^{-1}$. Concentrations related to optical rotation (c) are given in g/100 mL. thin layer chromatography (TLC) was carried out on 0.25 mm E. Merck® aluminium backed sheets coated with 60 $F_{254}$ silica gel. Visualization of the silica plates was achieved using a UV lamp (λmax = 254 nm) and/or by heating plates that were dipped in anisaldehyde solution or in ninhydrin solution. Flash chromatography was carried out on Scharlau® silica gel 60 Å (230-400 mesh) as the stationary, using forced flow of the mobile phase, which is specified in each experimental procedure.

### Compound characterization consideration

Although the name of products follows the IUPAC criteria, for clarity and comparative purpose, the numbering of protons and carbons in the NMR data is consistent with that corresponding to the sphingolipid numbering specified in the drawings of the corresponding structures.

### General Procedures

**General procedure for the *N*-amidation reaction of acids:** A solution of the corresponding acid (1.5 equiv.), hexafluorophosphate azabenzotriazole tetramethyl uranium (HATU) (1.5 equiv.) and *N,N*-diisopropylethylamine (DIPEA) (3.0 equiv.) were stirred at room temperature for approximately 45 min in $CH_2Cl_2$. This solution was added via syringe pump for 15 minutes into another solution of the amine in its hydrochloride form salt (1.0 equiv.) in $CH_2Cl_2$ cooled at 0 °C. The reaction was allowed to stir at room temperature and monitored by TLC until completion. Water was then added, both phases were separated, and the aqueous phase was extracted with $CH_2Cl_2$. The combined organic extracts were

dried over anhydrous $Na_2SO_4$, filtered, and concentrated under vacuum. The crude was purified by flash column chromatography on silica gel ($CH_2Cl_2$/MeOH/$NH_4OH$, 98:2:0.2).

**General procedure for the Boc deprotection of ceramides:** A solution of the Boc-protected ceramides (1 equiv.) in dry dioxane (0.2 mL) was cooled at 0 °C. Then a 4 M HCl solution in dioxane (12.3 equiv.) was added dropwise. The reaction was allowed to stir at room temperature and monitored by TLC until completion. The crude was purified by flash column chromatography on silica gel ($CH_2Cl_2$/MeOH/$NH_4OH$, 97:3:0.2).

**2-tridecylcycloprop-2-en-1-one (4)**

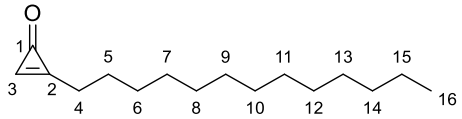


A mixture of NaI (2.519 g, 16.80 mmol, 2.2 equiv.) and 1-pentadecyne (2 mL, 7.62 mmol, 1 equiv.) was dissolved in dry THF (10.2 mL) under argon atmosphere in a Schlenck pressure tube. $TMSCF_3$ (5.63 mL, 38.09 mmol, 5 equiv.) was added, the Schlenck pressure tube was then sealed and the mixture was heated at 110 °C whit vigorous stirring. After 21 hours, the reaction was stopped upon addition of saturated aqueous $NaHCO_3$ solution. Both phases were separated, and the aqueous phase was extracted with $Et_2O$. The combined organic extracts were desiccated with anhydrous $MgSO_4$ and concentrated under vacuum to give a yellowish oily residue. The formation of the desired difluorocyclopropane was confirmed by $^1H$ NMR and $^{19}F$ NMR analysis.

The obtained crude difluorocyclopropane was dissolved in a hexane/AcOH (99:1) mixture and treated with silica at room temperature overnight. Afterwards, the mixture was filtered off under vacuum through a filter plate and the solution was extracted with sat. $NaHCO_3$ solution. The organic phase was dried over anhydrous $MgSO_4$ and concentrated under vacuum to give a yellowish oily residue. The residue was purified by flash column chromatography on silica gel (gradient: hexane/ethyl acetate, from 7:3 to 6:4) and finally the desired cyclopropenone was obtained as a white solid (1.724 g, 7.30 mmol, 96 % yield).

***R<sub>f</sub>*** = 0.20 (hexane/ethyl acetate, 1:1). **$^1$H NMR** (400 MHz, $CDCl_3$) δ in ppm: 8.40 (*s*, 1H, H-3), 2.64 (*t*, $J_{4,5}$ = 7.3 Hz, 2H, H-4), 1.68 (*app p.*, *J* = 7.4 Hz, 2H, H-5), 1.40-1.33 (*m*, 2H, H-6), 1.30-1.17 (*m*, 18H, from H-7 to H-15), 0.84 (*t*, $J_{16,15}$ = 6.6 Hz, 3H, H-16). **$^{13}$C NMR** (100 MHz, $CDCl_3$) δ in ppm: 170.3 (C-2), 158.0 (C-1), 148.2 (C-3), 32.0 ($CH_2$), 29.70 ($CH_2$), 29.68 (2 x $CH_2$), 29.6 ($CH_2$), 29.5 ($CH_2$), 29.4 ($CH_2$), 29.2 ($CH_2$), 29.0 (C-6), 27.5 (C-4), 25.7 (C-5), 22.7 ($CH_2$), 14.2 (C-16).

**6,6-Dimethyl-1-tridecyl-4,8-dioxaspiro[2.5]oct-1-ene (3)**

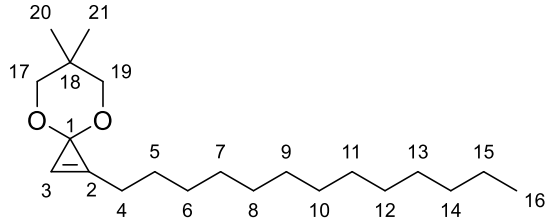

Tridecylcylopropenone **4** (1.005 g, 4.25 mmol, 1 equiv.) and $BF_4OEt_3$ (1.214 g, 6.39 mmol, 1.5 equiv.) were dissolved in dry $CH_2Cl_2$ (7 mL) under argon atmosphere, and the resulting mixture was vigorously stirred at room temperature for 30 min. Neopentylglycol (0.888 g, 8.53 mmol, 2 equiv.) and $Et_3N$ (1.18 mL, 8.47 mmol, 2 equiv.) dissolved in dry $CH_2Cl_2$ (2.3 mL) were then added over the previous mixture dropwise. The reaction mixture was then stirred at room temperature overnight.

After this time, the reaction was stopped with upon addition of sat. $NaHCO_3$ solution. The organic phase was washed multiple times with sat. $NaHCO_3$ solution, then, dried over $Na_2SO_4$ and concentrated under reduced pressure. A brown oily residue was obtained, which was purified by flash column chromatography on silica gel (hexane/AcOEt, 9:1) to give the desired cyclopropenone acetal as a yellow liquid (1.218 g, 3.78mmol, 89 % yield).

***R*$_f$** = 0.40 (hexane/ethyl acetate, 9:1). **$^1$H NMR** (400 MHz, $CDCl_3$) δ in ppm: 7.32 (*t*, $J_{3,4}$ = 1.2 Hz, 1H, H-3), 3.63 (*d*, $J_{gem}$ = 10.4 Hz, 2H, H-17 and H-19), 3.59 (*d*, $J_{gem}$ = 10.4 Hz, 2H, H-17' and H-19'), 2.52 (*td*, $J_{4,5}$ = 7.3 Hz, $J_{4-3}$ = 1.2 Hz, 2H, H- 4), 1.62 (*app p.*, *J* = 7.4 Hz, 2H, H-5), 1.40-1.25 (*m*, 20H, from H-6 to H-15), 1.06 (*s*, 3H, H-20), 1.00 (*s*, 3H, H-21), 0.88 (*t*, $J_{16,15}$ = 6.9 Hz, 3H, H-16). **$^{13}$C NMR** (100 MHz, $CDCl_3$) δ in ppm: 138.2 (C-2), 115.3 (C-3), 83.7 (C-1), 77.3 (C-17 and C-19), 32.1 ($CH_2$), 30.5 (C-18), 29.8 ($CH_2$), 29.8 ($CH_2$), 29.8 ($CH_2$), 29.7 ($CH_2$), 29.7 ($CH_2$), 29.5 ($CH_2$), 29.4 ($CH_2$), 29.3 ($CH_2$), 27.4 (C-5), 25.1 (C-4), 22.8 ($CH_2$), 22.6, 22.3 (C-20, C-21), 14.3 (C-16).

### *tert*-Butyl (*S*)-4-[(*R*)-(6,6-dimethyl-2-tridecyl-4,8-dioxaspiro[2.5]oct-1-en-1 yl)(hydroxy)methyl]-2,2-dimethyloxazolidine-3-carboxylate (2)

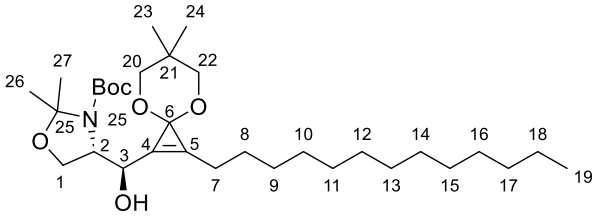


Cyclopropenone acetal **3** (0.609 g, 1.89 mmol, 1.8 equiv.) and HMPA (0.66 mL, 3.79 mmol, 3.06 equiv.) were dissolved in dry THF (8.5 mL) under argon atmosphere. The solution was cooled down to -55 °C and BuLi (0.75 mL, 2.5 M in hexanes, 1.88 mmol, 1.8 equiv.) was added dropwise. The mixture was stirred for 30 min and then *(S)*-Garner's aldehyde (0.234 g, 1.05 mmol, 1 equiv.) dissolved in dry THF (1.9 mL) was added. The resulting mixture was stirred at -55 °C overnight.

Aqueous sat. $NH_4Cl$ sol. was then added, both phases were separated, and the aqueous phase was extracted with DCM. The combined organic extracts were dried over anhydrous $Na_2SO_4$, filtered and concentrated under vacuum to give a brownish residue which was purified by flash column chromatography on silica gel (hexane/AcOEt, 8:2). Finally, the desired addition product **3** was obtained as a colourless liquid (0.438 g, 0.793 mmol, 76 % yield).

***R*$_f$ =** 0.17 Hexane/AcOEt (8:2). **$^1$H NMR** δ in ppm (400 MHz, $CDCl_3$, 50 °C): 5.04-5.03 (*m*, 1H, H-3), 4.16 (*br s*, 1H, H-2), 4.00-3.99 (*m*, 2H, H-1), 3.69-3.64 (*m*, 2H, H-20 and H-22), 3.56 (*d*, $J_{gem}$ = 11.0 Hz, 2H, H- 20' and H-22'), 2.47 (*t*, $J_{7,8}$ = 7.5 Hz, 2H, H-7), 1.65-1.57 (*m*, 6H, isopropylidene), 1.50 (*s*, 9H, *tert*-butyl), 1.37-1.26 (*m*, 22H, from H-8 to H-18), 1.06 (*s*, 3H,

H-23), 0.94 (*s*, 3H, H-24), 0.88 (*t*, $J_{19,18}$ = 6.7 Hz, 3H, H-19). **$^{13}$C NMR** δ in ppm (100 MHz, $CDCl_3$): 154.0 (Boc carbonyl), 130.1 (C-5), 128.7 (C-4), 95.0 (isopropylidene quaternary C), 84.9 (C-6), 81.3 (Boc quaternary C), 77.7 (C-20), 77.2 (C-22), 68.5 (C-3), 64.8 (C-1), 61.4 (C-2), 32.0 ($CH_2$), 30.4 (C-21), 29.8 ($CH_2$), 29.8 ($CH_2$), 29.8 ($CH_2$), 29.8 ($CH_2$), 29.7 ($CH_2$), 29.5 ($CH_2$), 29.5 ($CH_2$), 29.4 ($CH_2$), 28.5 (Boc Me groups), 27.7 (C-8), 26.2 (isopropylidene Me groups), 24.5 (C-7), 22.8 ($CH_2$), 22.6 (C-23), 22.2 (C-24), 14.3 (C-19).

**2-*[(1R,2S)*-2-Amino-1,3-dihydroxypropyl]-3-tridecylcycloprop-2-en-1-one (4)**

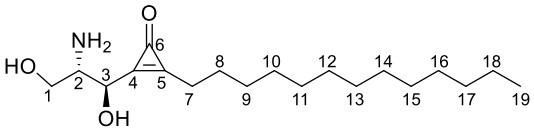


Addition product **2** (0.170 g, 0.31 mmol, 1 equiv.) was dissolved in dioxane (8 mL) and HCl (7.4 mL, 4M in dioxane, 29.5 mmol, 96 equiv.) was added dropwise. After the addition the reaction mixture was warmed up to room temperature and stirred for 3 h. The mixture was then concentrated under vacuum to obtain the desired aminodiol hydrochloride salt **1-Cl salt** as a brown solid.

Aminodiol hydrochloride salt **1-Cl salt** was neutralized and purified by flash column chromatography on silica gel $CH_2Cl_2$/MeOH/$NH_4OH$ (95:5:1) to furnish the aminodiol **1** as a white solid (0.171 g, 0.473 mmol, 64% yield).

***R*$_f$** = 0.20 DCM/MeOH/$NH_4OH$ (9:1:0.1). **$^1$H NMR** δ in ppm (400 MHz, $CD_3OD$): 4.75 (*dt*, $J_{3,2}$ = 5.5 Hz, $J_{3,7}$ = 1.0 Hz, 1H, H-3), 3.66 (*dd*, $J_{1,1'}$ = 11.0 Hz, $J_{1,2}$ = 5.5 Hz, 1H, H-1), 3.61 (*dd*, $J_{1',1}$ = 11.0 Hz, $J_{1',2}$ = 5.5 Hz, 1H, H-1'), 3.09 (*app q*, $J_{2,1}$ = $J_{2,1'}$ = $J_{2,3}$ = 5.5 Hz, 1H, H-2), 2.74 (*td*, $J_{7,8}$ = 7.2 Hz, $J_{7,3}$ = 1.0 Hz, 2H, H-7), 1.75 (*p*, $J_{8,7}$ = $J_{8,9}$ = 5.5 Hz, 2H, H-8), 1.46-1.26 (*m*, 20H, from H-9 to H-18), 0.90 (*t*, $J_{19,18}$ = 7.0 Hz, 3H, H-19); **$^{13}$C NMR** δ in ppm (100 MHz, $CD_3OD$): 162.8 (C-6), 162.0 (C-4), 161.2 (C-5), 71.3 (C-3), 63.6 (C-1), 57.6 (C-2), 33.1 ($CH_2$), 30.9 ($CH_2$), 30.8 (3 x $CH_2$), 30.6 ($CH_2$), 30.5 ($CH_2$), 30.4 ($CH_2$), 30.3 ($CH_2$), 27.4 (C-8), 26.8 (C-7), 23.8 ($CH_2$), 14.5 (C-19).

***tert*-Butyl-(*21R*)-4,4-difluoro-2-[(*1R,2S*)-1,3-dihydroxy-1-(3-oxo-2-tridecylcycloprop-1-en-1-yl)propan-2-yl]carbamoyl]-pyrrolidine-1-carboxylate (PR280-7Boc)**

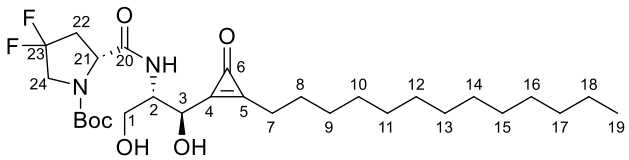


Addition product **2** (0.170 g, 0.31 mmol, 1 equiv.) was dissolved in dioxane (8 mL) and HCl (7.4 mL, 4M in dioxane, 29.5 mmol, 96 equiv.) was added dropwise. After the addition the reaction mixture was warmed up to room temperature and stirred for 3 h. The mixture was then concentrated under vacuum to obtain the desired aminodiol hydrochloride salt **1-Cl salt** as a brown solid (99% yield based on NMR using benzyl ether as the internal standard), which was used without further purification.

The acylation reaction was performed as described in the general procedure for the *N*-amidation reaction of acids by using (*R*)-1-(*tert*-butoxycarbonyl)-4,4-difluoropyrrolidine-2-carboxylic acid (0.105 g, 0.42 mmol, 1.5 equiv.), HATU (0.160 g, 0.42 mmol, 1.5 equiv.), DIPEA (0.15 mL, 0.84 mmol, 3.0 equiv.) and crude aminodiol hydrochloride salt **1-Cl salt**

(0.101 g, 0.28 mmol, 1 equiv.) in dry $CH_2Cl_2$ (25.8 mL). The resulting product was obtained as a yellow oil (0.062 g, 0.11 mmol, 38 % yield over the two steps).

**$R_f$** = 0.57 (9:1 DCM/MeOH). **[α]$^{25}_D$** 20 (*c* 0.12, *$CD_3OH$*). **$^1$H NMR** (400 M Hz, *$CD_3OD$*, δ in ppm): 4.91 (*d*, $J_{3,2}$ = 6.5 Hz, 1H, H-3), 4.44 (*m*, 1H, H-21), 4.16 (*dt*, $J_{2,3}$ = 6.5 Hz, $J_{2,1}$ = $J_{2,1'}$ = 5.3 Hz, 1H, H-2), 3.81 (*m*, 2H, H-22), 3.71 (*m*, 2H, H-1), 2.73 (*t*, $J_{7,8}$ = 7.3 Hz, 2H, H-7), 2.62 (*m*, 2H, H-24), 1.75 (*p*, $J_{8,7}$ = $J_{8,9}$ = 7.3 Hz, 2H, H-8), 1.47 (*s*, 9H, H-9, *tert*-butyl), 1.29 (*s*, 20H, from H-9 to H-18), 0.89 (*m*, 3H, H-19). **$^{13}$C NMR** (100 MHz, *$CD_3OD$*), δ in ppm) δ = 173.4 (C-20), 162.7 (C-6), 161.4 (C-4), 160.6 (C-5), 155.9 (Boc carbonyl), 130.9 (*t*, $J_{23,F}$ = 320.4 Hz, C-23), 82.7 (Boc quaternary C), 68.7 (C-3), 61.1 (C-1), 59.4 (C-21), 56.1 (C-2), 54.6 (*m*, $J_{24,F}$ = 30.7 Hz, C-24), 38.7 (app t, $J_{22,F}$ = 26.6 Hz, C-22), 33.1 (C-17), 30.8 ($CH_2$), 30.7 (2 x $CH_2$), 30.6 ($CH_2$), 30.5 ($CH_2$), 30.4 ($CH_2$), 30.3 ($CH_2$), 30.2 ($CH_2$), 28.6 ($CH_3$, *tert*-butyl), 27.4 (C-7), 26.7 (C-8), 23.7 ($CH_2$), 14.4 (C-19). **$^{19}$F NMR** (400 MHz, *$CD_3OD$*, δ in ppm): -100.2 (*dp*, $J_{F,F'}$ = 232.3 Hz, $^3J_{F,H}$ = 16.4 Hz, F), -101.7 (*app dp*, $J_{F',F}$ = 232.3 Hz, $^3J_{F',H}$ = 16.4 Hz, F'). **HRMS ESI-*T*OF** [M+H]$^+$ $C_{29}H_{49}F_2N_2O_6^+$ calc for 559,3552 found for 559,3560. **F*T*-IR (A*T*R)** ν in cm$^{-1}$: 3334, 2924, 2853, 2504, 1845, 1683, 1623, 1457, 1395, 1367, 1160, 1099, 935, 849, 771, 508.

**_N_-[(_1R,2S_)-1,3-dihydroxy-1-(3-oxo-2-tridecylcycloprop-1-en-1-yl)propan-2-yl]-(_21R_)-4,4-difluoropyrrolidine-2-carboxamide (PR280-7)**

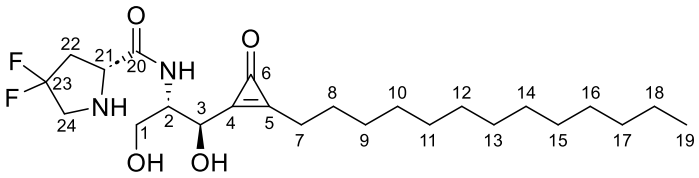


The reaction was performed as described in the general procedure for the Boc deprotection of ceramides by using **PR280-7Boc** (0.066 g, 0.12 mmol, 1 equiv.), HCl 4N in dioxane (0.36 mL, 1.45 mmol, 12 equiv.) in 0.2 mL dioxane. After 3 hours, the reaction was quenched and purification of the reaction crude by flash column chromatography afforded the desired product as a white solid (0.030 g, 0.065 mmol, 21% yield over the three steps).

**$R_f$** = 0.31 (9:1 DCM/MeOH). **[α]$^{25}_D$** 14 (*c* 0.2, *$CD_3OH$*). **$^1$H NMR** (400 M Hz, *$CD_3OD$*, δ in ppm): 4.87 (*m*, 1H, H-3), 4.06 (*m*, 1H, H-2), 3.94 (*t*, $J_{21,22}$ = 8.3 Hz, 1H, H-21), 3.85 (*dd*, $J_{1,1'}$ = 11.2 Hz, $J_{1,2}$ = 4.5 Hz, 2H, H-1), 3.70 (*dd*, $J_{1',1}$ = 11.2 Hz, $J_{1',2}$ = 4.5 Hz, 2H, H-1'), 3.23 (*m*, 2H, H-24), 2.72 (*td*, $J_{7,8}$ = 7.3 Hz, $J_{7,3}$ = 1.1 Hz, 2H, H-7), 2.50 (*m*, 2H, H-22), 1.75 (*p*, $J_{8,7}$ = $J_{8,9}$ = 7.3 Hz, 2H, H-8), 1.43 (*m*, 2H, H-9), 1.29 (*s*, 18H, from H-10 to H-18), 0.90 (*m*, 3H, H-19). **$^{13}$C NMR** (100 MHz, *$CD_3OD$*), δ in ppm) δ = 175.3 (C-20), 162.5 (C-6), 162.2 (C-4), 160.6 (C-5), 132.2 (*t*, $J_{23,F}$ = 247.0 Hz, C-23), 68.9 (C-3), 61.2 (C-1), 59.7 (C-21), 55.2 (C-2), 53.9 (*t*, $J_{24,F}$ = 28.6 Hz, C-24), 39.1 (*t*, $J_{22,F}$ = 25.5 Hz, C-22), 33.1 ($CH_2$), 30.8 ($CH_2$), 30.7 (2 x $CH_2$), 30.6 ($CH_2$), 30.5 ($CH_2$), 30.4 ($CH_2$), 30.3 ($CH_2$), 30.3 ($CH_2$), 27.5 (C-8), 26.6 (C-7), 23.7 ($CH_2$), 14.4 (C-19). **$^{19}$F NMR** (400 MHz, *$CD_3OD$*, δ in ppm): -100.3 (*app dpq*, $J_{F,F'}$ = 230.0 Hz, $^3J_{F,H}$ = 18.8 Hz, $^4J_{F,H}$ = 5.1 Hz, F), -107.4 (*app dsext*, $J_{F',F}$ = 230.0 Hz, $^4J_{F',H}$ = 5.1 Hz, F'). **HRMS ESI-*T*OF** [M+H]$^+$ $C_{24}H_{41}F_2N_2O_4^+$ (m/z): calc for 459,3028 found for 459,3029. **F*T*-IR (A*T*R)** ν in cm$^{-1}$: 3.332, 3.290, 2.956, 2.917, 2.848, 1.833, 1.662, 1.608, 1.550, 1.362, 1.288, 1.262, 1.162, 1.070, 1.061, 705, 623.

### *tert*-Butyl-2-[((*1R,2S)*-1,3-dihydroxy-1-(3-oxo-2-tridecylcycloprop-1-en-1-yl)propan-2-yl)carbamoyl]-6,7-dihydrothiazolo[5,4]pyridine-5(4*H*)-carboxylate (PR280-1Boc)

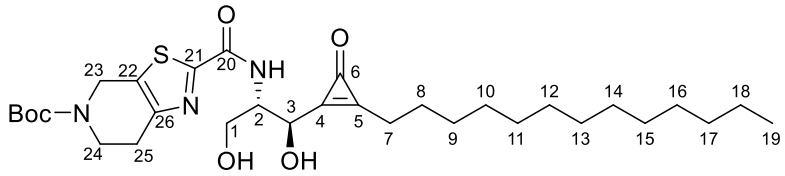

Addition product **2** (0.170 g, 0.31 mmol, 1 equiv.) was dissolved in dioxane (8 mL) and HCl (7.4 mL, 4M in dioxane, 29.5 mmol, 96 equiv.) was added dropwise. After the addition the reaction mixture was warmed up to room temperature and stirred for 3 h. The mixture was then concentrated under vacuum to obtain the desired aminodiol hydrochloride salt **1-Cl salt** as a brown solid (99% yield based on NMR using benzyl ether as the internal standard), which was used without further purification.

The acylation reaction was performed as described in the general procedure for the *N*-amidation reaction of acids by using 5-(*ter0t*-butoxycarbonyl)-4,5,6,7-tetrahydrothiazolo[5,4]pyridine-2-carboxylic acid (0.105 g, 0.37 mmol, 1.5 equiv.), HATU (0.137 g, 0.36 mmol, 1.5 equiv.), DIPEA (135.8 µL, 0.78 mmol, 3.0 equiv.) and aminodiol hydrochloride salt **1-Cl salt** (0.026 g, 0.24 mmol, 1 equiv.) in dry $CH_2Cl_2$ (21.8 mL). The resulting product was obtained as a yellow oil (0.024 g, 0.041 mmol, 57 % yield over the two steps).

**$R_f$** = 0.37 (9:1 $CH_2Cl_2$/MeOH). $[\alpha]^{25}_D$ 24 (*c* 0.2, *$CD_3OH$*). **$^1$H NMR** (400 M Hz, *$CD_3OD$*, δ in ppm: 4.97 (*d*, $J_{3,2}$ = 8.0 Hz, 1H, H-3), 4.72 (*s*, 2H, H-23), 4.28 (*ddd*, $J_{2,3}$ = 8.0 Hz, $J_{2,1}$ = 5.0 Hz, $J_{2,1'}$ = 4.2 Hz,1H, H-2), 3.95 (*dd*, $J_{1,1'}$ = 11.3 Hz, $J_{1,2}$ = 5.0 Hz, 1H, H-1), 3.82 (m, 1H, H-1'), 3.77 (*t*, $J_{24,25}$ = 5.8 Hz, 2H, H-24), 2.89 (*t*, $J_{25,24}$ = 5.8 Hz, 2H, H-25), 2.66 (*t*, $J_{7,8}$ = 7.1 Hz, 2H, H-7), 1.68 (*p*, $J_{8,7}$ and $J_{8,9}$ = 7.1 Hz, 2H, H-8), 1.49 (*s*, 9H, H-9, *tert*-butyl), 1.28 (s, 20H, from H-9 to H-18), 0.90 (*m*, 3H, H-19). **$^{13}$C NMR** (100 MHz, *$CD_3OD$*, δ in ppm): 175.9 (C-20), 162.6 (C-21), 162.0 (C-6), 161.6 (C-4), 160.6 (C-5), 156.1 (Boc carbonyl), 151.9 (C-26), 133.6 (C-22), 81.9 (Boc quaternary C), 68.8 (C-3), 61.2 (C-1), 55.6 (C-2), 43.0 (C-23), 41.8 (C-24), 33.1 ($CH_2$), 30.8 (2 x $CH_2$), 30.7 (2 x $CH_2$), 30.5 ($CH_2$), 30.4 ($CH_2$), 30.3 ($CH_2$), 30.2 ($CH_2$), 28.6 ($CH_3$, *tert*-butyl), 27.9 (C-25), 27.4 (C-8), 26.8 (C-7), 23.7 ($CH_2$), 14.5 (C-19). **HRMS ESI-*T*OF** $[M+H]^+$ $C_{31}H_{50}N_3O_6S^+$ (m/z): calc for 592,3414 found for 592,3412. **F*T*-IR (A*T*R)** ν in $cm^{-1}$: 3330, 2923, 2852, 2362, 2338, 2021, 1845, 1699, 1654, 1541, 1508, 862, 467, 412.

### *N*-[*(1R,2S)*-1,3-dihydroxy-1-(3-oxo-2-tridecylcycloprop-1-en-1-yl)propan-2-yl]-4,5,6,7-tetrahydrothiazolo[5,4]pyridine-2-carboxamide (PR280-1)

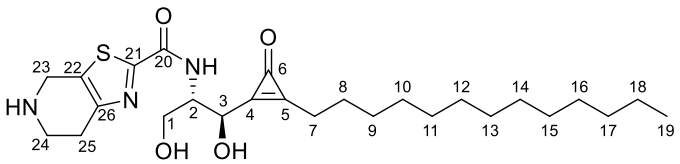

The reaction was performed as described in general procedure for the Boc deprotection of ceramides by using **PR280-1Boc** (0.042 g, 0.072 mmol, 1 equiv.), HCl 4N in dioxane (0.21 mL, 0.86 mmol, 12 equiv.) in 0.2 mL dioxane. After 3 hours the reaction was quenched and purification of the reaction crude by flash column chromatography afforded the desired product as a yellow crystal (0.026 g, 0.053 mmol, 41% yield over the three steps).

**$R_f$** = 0.1 (9:1 $CH_2Cl_2$/MeOH). **[α]$^{25}_D$** 28 (*c* 0.2, *$CD_3OH$*). **$^1$H NMR** (400 M Hz, *$CD_3OD$*, δ in ppm: 4.96 (*d*, $J_{3,2}$ = 8.1 Hz, 1H, H-3), 4.28 (*m*, 1H, H-2), 4.08 (*s*, 2H, H-23), 3.94 (*dd*, $J_{1,1'}$ = 11.3 Hz, $J_{1,2}$ = 5.1 Hz, 1H, H-1), 3.82 (*dd*, $J_{1';1}$ = 11.3, $J_{1';2}$ = 4.3 Hz, 1H, H-1'), 3.16 (*m*, 2H, H-24), 2.88 (*t*, $J_{25,24}$ = 5.9 Hz, 2H, H-25), 2.66 (*t*, $J_{7,8}$ = 7.8 Hz, 2H, H-7), 1.69 (*p*, $J_{8,7}$ and $J_{8,9}$ = 7.8 Hz, 2H, H-8), 1.29 (s, 20H, from H-9 to H-18), 0.90 (*m*, 3H, H-19). **$^{13}$C NMR** (100 MHz, *$CD_3OD$*, δ in ppm): 162.6 (C-20), 162.0 (C-21), 161.8 (C-6), 161.1 (C-4), 160.0 (C-5). 151.8 (C-26), 135.2 (C-22), 68.8 (C-3), 61.2 (C-1), 55.6 (C-2), 44.1 (C-23), 43.8 (C-24), 33.1 ($CH_2$), 30.8 (2 x $CH_2$), 30.7 (2 x $CH_2$), 30.5 ($CH_2$), 30.4 ($CH_2$), 30.3 ($CH_2$), 30.2 ($CH_2$), 28.3 (C-25), 27.4 (C-8), 26.8 (C-7), 23.7 ($CH_2$), 14.5 (C-19). **HRMS ESI-*TOF*** $[M+H]^+$ $C_{26}H_{42}N_3O_4S^+$ (m/z): calc for 492,2890 found for 492,2891. **F*T*-IR (A*T*R)** ν in $cm^{-1}$: 3282, 2920, 2851, 1841, 1651, 1622, 1539, 1518, 1456, 1434, 1363, 1091, 1051, 907, 847, 809, 719, 643, 546, 417.

### *N*-[*(1R,2S)*-1,3-dihydroxy-1-(3-oxo-2-tridecylcycloprop-1-en-1-yl)propan-2-yl]isoquinoline-3-carboxamide (PR280-3)

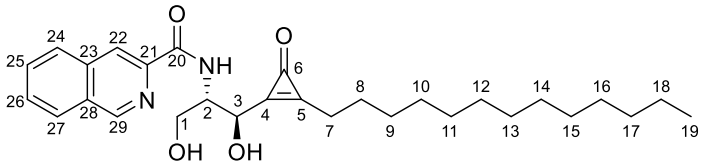


Addition product **2** (0.170 g, 0.31 mmol, 1 equiv.) was dissolved in dioxane (8 mL) and HCl (7.4 mL, 4M in dioxane, 29.5 mmol, 96 equiv.) was added dropwise. After the addition the reaction mixture was warmed up to room temperature and stirred for 3 h. The mixture was then concentrated under vacuum to obtain the desired aminodiol hydrochloride salt **1-Cl salt** as a brown solid (99% yield based on NMR using benzyl ether as the internal standard), which was used without further purification**.**

The acylation reaction was performed as described in the general procedure for the *N*-amidation reaction of acids by using isoquinoline-3-carboxylic acid (0.045 g, 0.26 mmol, 1.5 equiv.), HATU (0.134 g, 0.35 mmol, 1.5 equiv.), DIPEA (0.13 mL, 0.70 mmol, 3.0 equiv.) and aminodiol hydrochloride salt **1-Cl salt** (0.085 g, 0.24 mmol, 1 equiv.) in dry $CH_2Cl_2$ (21 mL). The resulting product was obtained as red oil (0.058 g, 0.122 mmol, 52 % yield over the two steps).

**$R_f$** = 0.57 (9:1 $CH_2Cl_2$/MeOH). **[α]$^{25}_D$** 30 (*c* 0.4, *$CD_3OH$*). **$^1$H NMR** (400 M Hz, *$CD_3OD$*, δ in ppm): 9.24 (*s*, 1H, H-29), 8.50 (*s*, 1H, H-22), 8.12 (*dd*, $J_{27,26}$ = 8.1 Hz, $J_{27,25}$ = 1.4 Hz, 1H, H-27), 8.02 (*dd*, $J_{24-25}$ = 8.1 Hz, $J_{24,26}$ = 1.3 Hz, 1H, H-24), 7.82 (*ddd*, $J_{25,24}$ = 8.1 Hz, $J_{25,26}$ = 6.9 Hz, $J_{25,27}$ = 1.4 Hz, 1H, H-25), 7.76 (*ddd*, $J_{26,27}$ = 8.1 Hz, $J_{26,25}$ = 6.9 Hz, $J_{26,24}$ = 1.3 Hz, 1H, H-26), 5.04 (*d*, $J_{3,2}$ = 7.6 Hz, 1H, H-3), 4.43 (*dt*, $J_{2,3}$ = 7.6 Hz, $J_{2,1}$ = 4.5 Hz, 1H, H-2), 4.04 (*dd*, $J_{1,1'}$ = 11.3 Hz, $J_{1,2}$ = 4.5 Hz, 1H, H-1), 3.86 (*dd*, $J_{1';1}$ = 11.3 Hz, $J_{1';2}$ = 4.5 Hz, 1H, H-1'), 2.61 (*t*, $J_{7,8}$ = 7.5 Hz, 2H, H-7), 1.62 (*p*, $J_{8,7}$ = 7.5 Hz, $J_{8,9}$ = 7.5 Hz, 2H, H-8), 1.25 (*s*, 20H, from H-9 to H-18), 0.88 (*m*, 3H, H-19). **$^{13}$C NMR** (100 MHz, *$CD_3OD$*), δ in ppm): 167.1 (C-20), 162.5 (C-6), 162.1 (C-4), 160.8 (C-5), 152.8 (C-29), 144.3 (C-21), 137.2 (C-23), 132.5 (C-25), 131.3 (C-28), 130.5 (C-26),129.1 (C-24), 128.9 (C-27), 121.6 (C-22), 69.0 (C-3), 61.4 (C-1), 55.5 (C-2), 33.0 ($CH_2$), 30.9 ($CH_2$), 30.8 (2 x $CH_2$), 30.6 ($CH_2$), 30.5 ($CH_2$), 30.4 ($CH_2$), 30.3 ($CH_2$), 30.2 ($CH_2$), 27.3 (C-8) 26.8 (C-7), 23.7 ($CH_2$), 14.4 (C-19). **HRMS ESI-*TOF*** $[M+H]^+$ $C_{30}H_{40}N_2O_4^+$ (m/z): calc for 481,3060 found for 481,3060. **F*T*-IR (A*T*R)** ν in $cm^{-1}$: 3356, 2922, 2851, 1843, 1653, 1623, 1518, 1465, 1437, 1051, 766, 745, 639, 496.

**Toxicity of reagents and solvents used:**

***Table 4:*** *Toxicity of reagents and solvents used.*

| Reagent/solvent | Purity (%) and/or concentration | Toxicity | Manipulation |
|---|---|---|---|
| NaI | 99 | GHS07, GHS08, GHS09 | Solid residues/ aqueous solutions |
| AcOH | 99.99 | GHS02, GHS05 | Aqueous solutions |
| $SiO_2$ | 100 | - | Dirty silica residues |
| Neopentylglicol | 98 | GHS07 | Solid residues |
| $NEt_3$ | 100 | GHS02, GHS05, GHS06, GHS08 | Non-halogenated organic residues |
| $BF_4OEt_3$ | 97 | GHS02, GHS05 | Solid residues |
| BuLi | 1.6 M in hexanes | GHS02, GHS05, GHS07, GHS08, GHS09 | Neutralization with $H_2O$, then disposed at aqueous solutions |
| HMPA | 99 | GHS05, GHS08 | Non-halogenated organic residues |
| HATU | 99.98 | GHS02, GHS07 | Solid residues |
| DIPEA | 100 | GHS02, GHS05, GHS06 | Non-halogenated organic residues |
| HCl | 37 (w/w) 4M in dioxane | GHS05, GHS07 | Neutralization with $H_2O$, then disposed at aqueous solutions |
| $Boc_2O$ | 98 | GHS02, GHS05, GHS06 | Solid residues |
| $CH_2Cl_2$ | 100 | GHS07, GHS08 | Halogenated organic residues |
| MeOH | 100 | GHS02, GHS06, GHS08 | Non-halogenated organic residues |
| AcOEt | 100 | GHS02, GHS07 | Non-halogenated organic residues |
| Hexane | 100 | GHS02, GHS07, GHS08, GHS09 | Non-halogenated organic residues |
| Dioxane | 100 | GHS02, GHS07, GHS08 | Non-halogenated organic residues |
| THF | 100 | GHS02, GHS07, GHS08 | Non-halogenated organic residues |

All chemical residues are stored in a safety cabinet equipped with an air filtration system and are collected monthly for proper disposal in accordance with environmental safety regulations.

## 5. Conclusions

This project successfully developed and optimized a multi-step synthetic strategy to obtain three new ceramide analogues—**PR280-1**, **PR280-3**, and **PR280-7**—designed as potential inhibitors of Des1. These compounds were selected based on prior docking studies predicting improved activity and selectivity compared to **PR280**.

The key synthetic challenge involved the protection and functionalization of a cyclopropenone scaffold, followed by a stereoselective addition to (*S*)-Garner's aldehyde and a final *N*-acylation step. Special emphasis was placed on optimizing reaction conditions, particularly for the deprotection and amidation stages. Notably, the aminodiol intermediate in its hydrochloride salt form (**1-Cl salt**) was shown to be significantly more stable than its neutral counterpart and was therefore used directly in amidation reactions.

Yields for the overall synthetic routes were 33 % for **PR280-3** (5 steps), 26 **%** for **PR280-1** (6 steps), and 13 % for **PR280-7** (7 steps). Structural confirmation of the final compounds was achieved through comprehensive spectroscopic analysis, including $^{1}H$ and $^{13}C$ NMR, COSY, HSQC, HRMS, and IR.

The synthesized analogues represent promising new candidates for future biological evaluation as Des1 inhibitors, that will be conducted in the coming days, contributing to the development of new tools for potential anticancer therapies targeting sphingolipid metabolism.

# Annexes

**PR280-7Boc:**

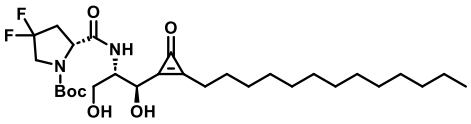


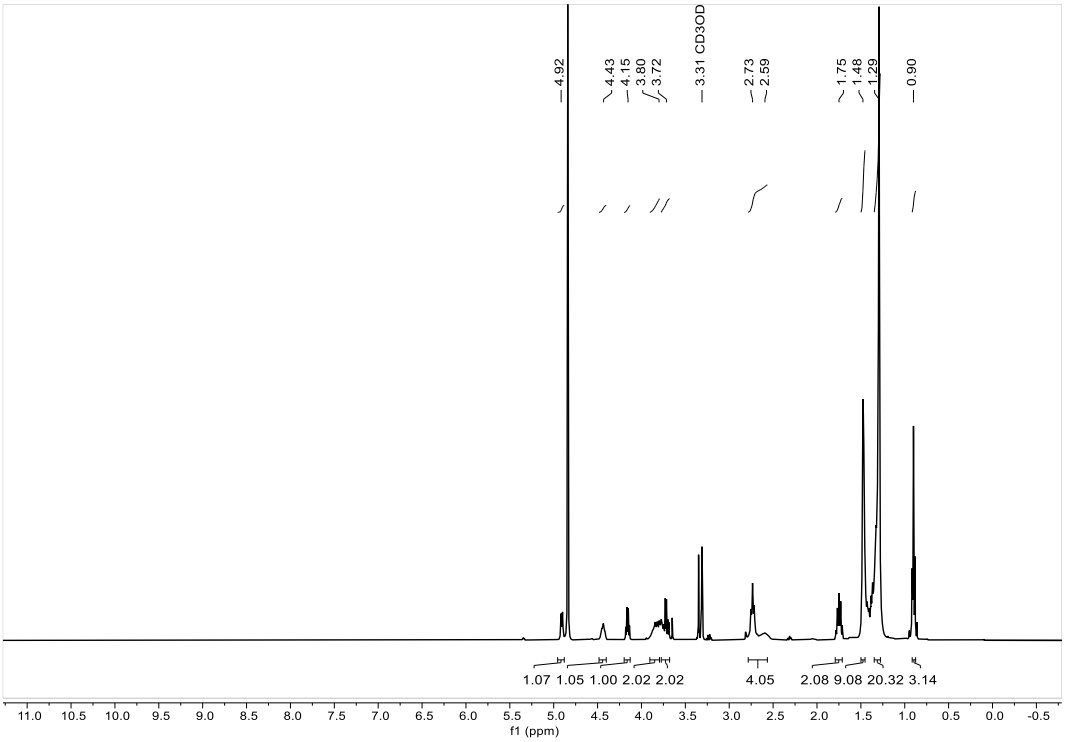


***Figure 11:*** *$^{1}$H NMR spectrum of* ***PR280-7Boc.***

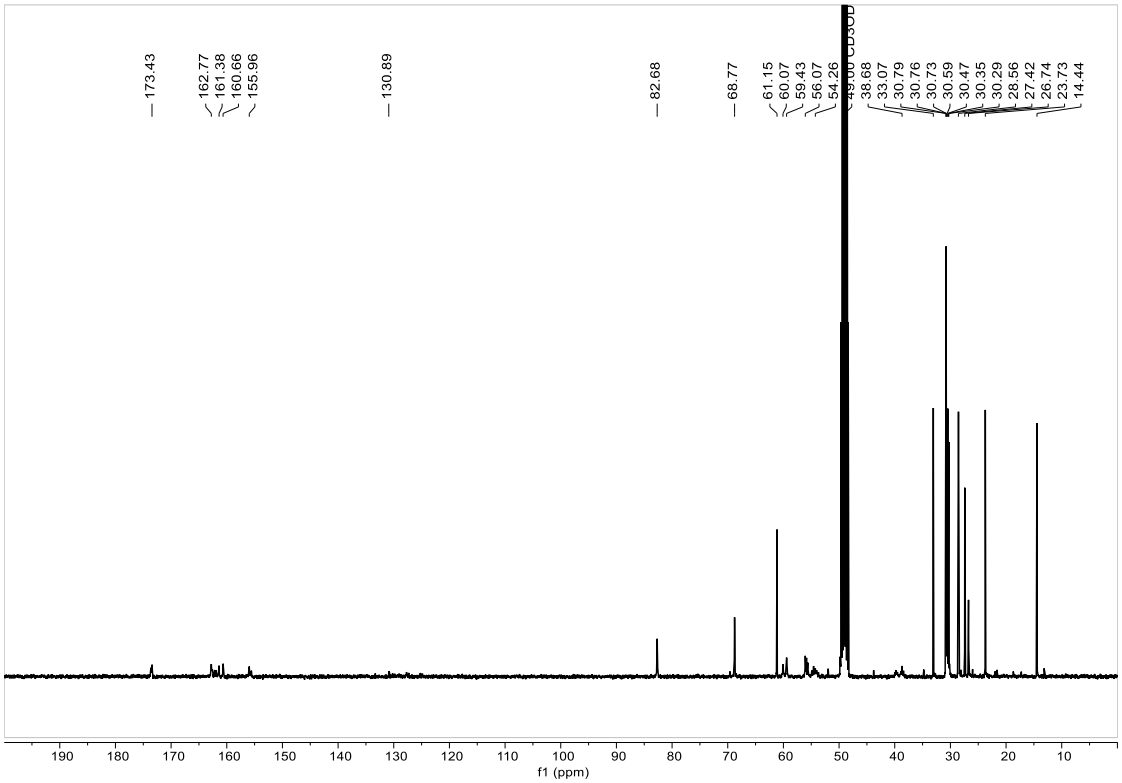


***Figure 12:*** *$^{13}$C NMR spectrum of* ***PR280-7Boc.***

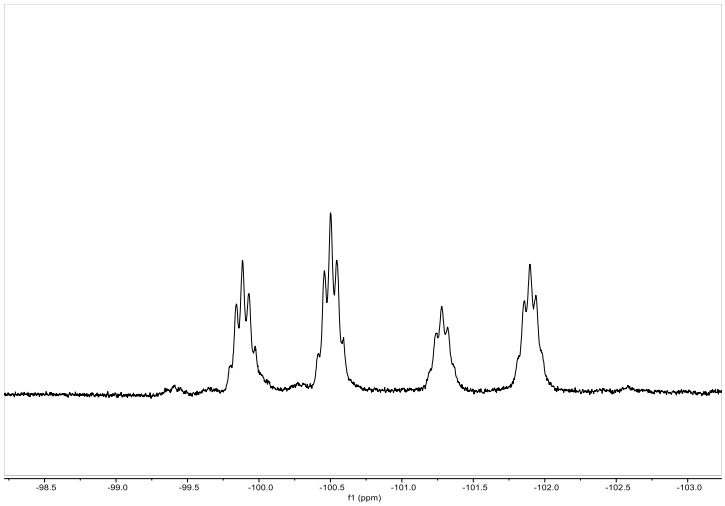


***Figure 13:*** *$^{19}$F NMR spectrum of* ***PR280-7Boc.***

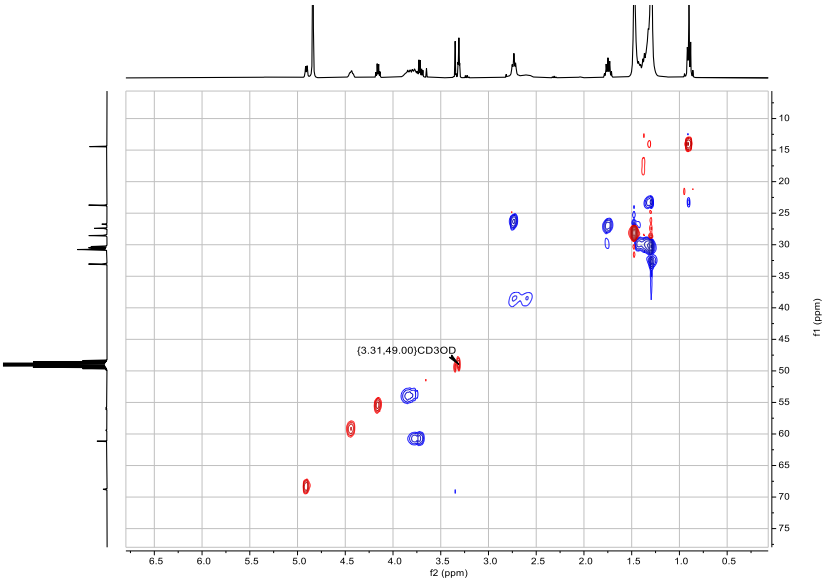


***Figure 14:*** *HSQC NMR spectrum of* ***PR280-7Boc.***

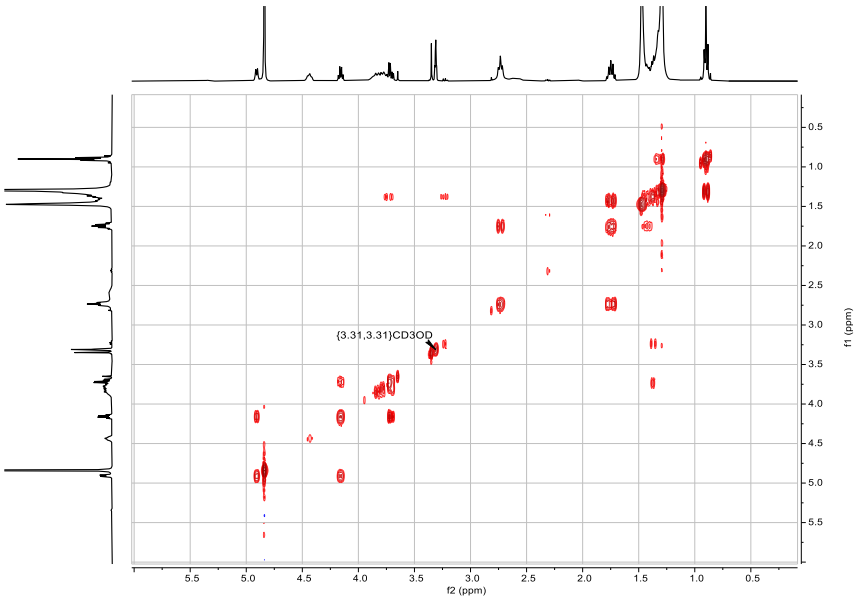


***Figure 15:*** *COSY spectrum of* ***PR280-7Boc.***

**PR280-7:**

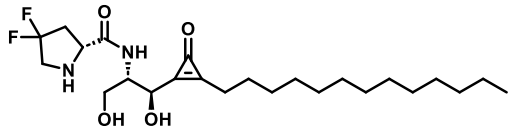

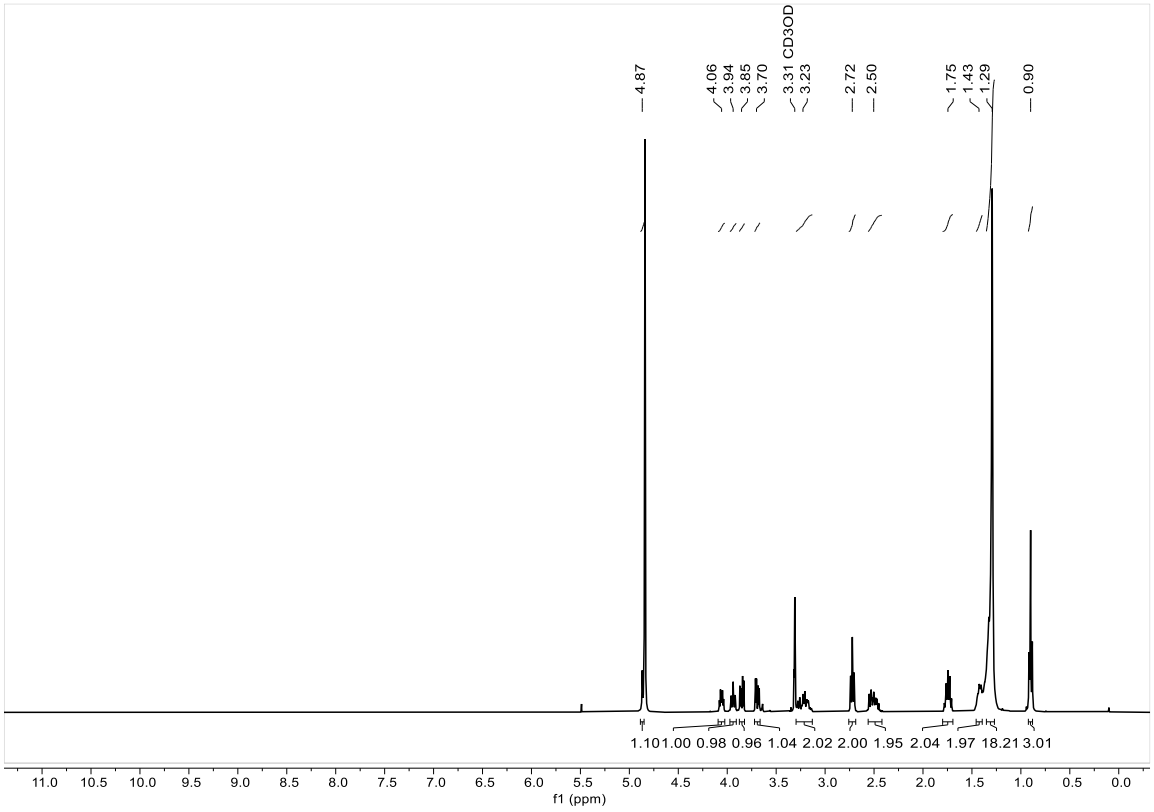


***Figure 16:*** *$^{1}$H NMR spectrum of* ***PR280-7.***

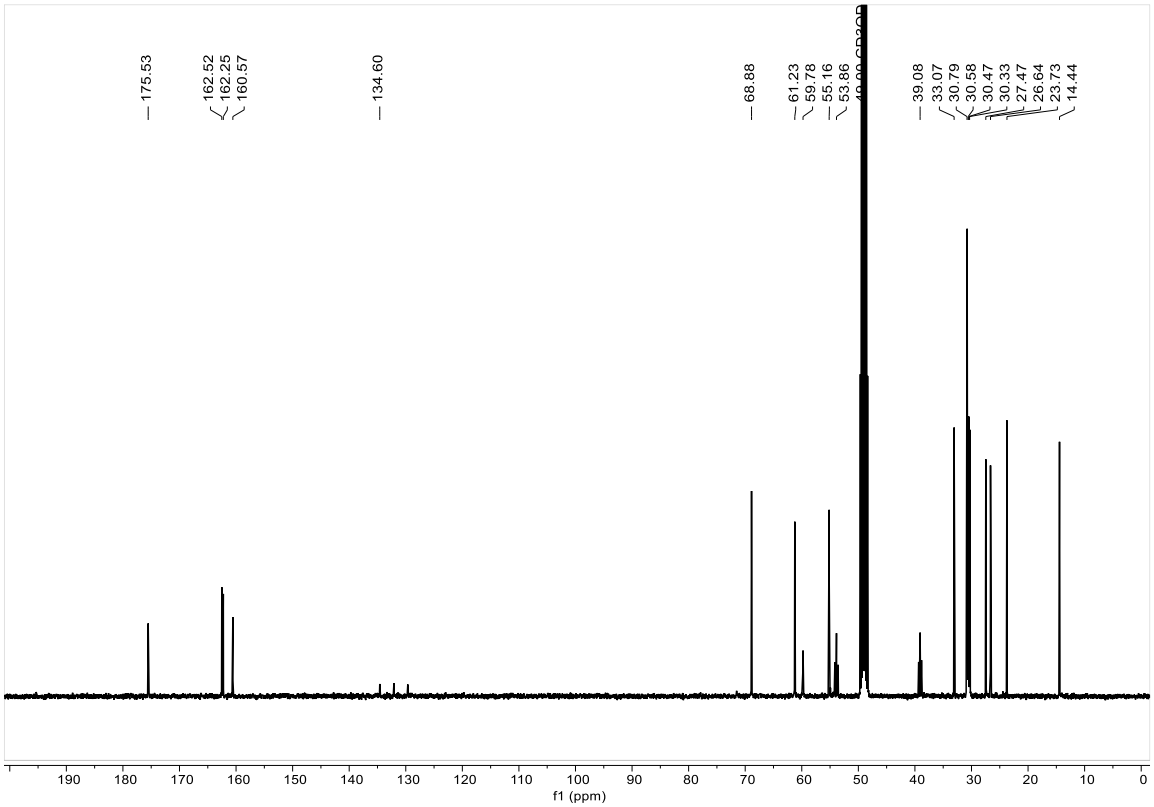


***Figure 17:*** *$^{13}$C NMR spectrum of* ***PR280-7.***

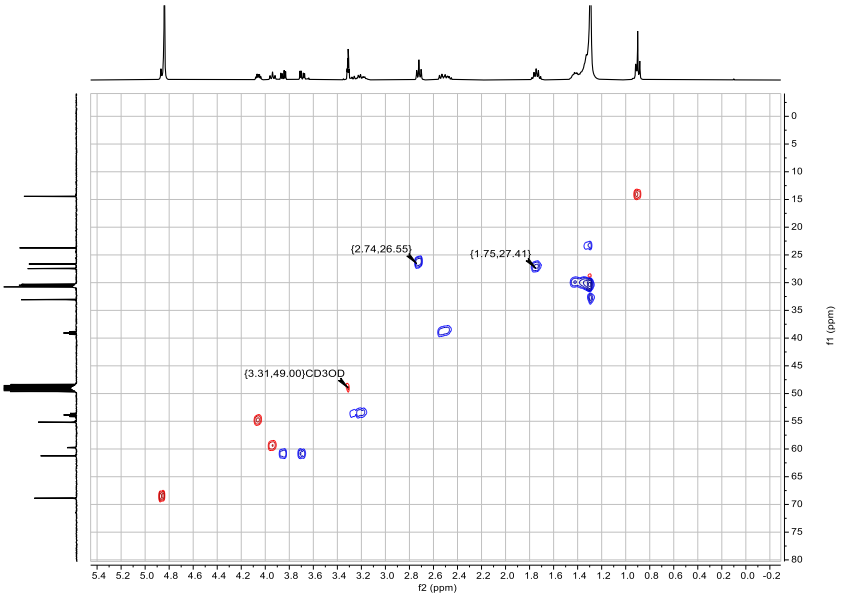


***Figure 18:*** *HSQC NMR spectrum of* ***PR280-7.***

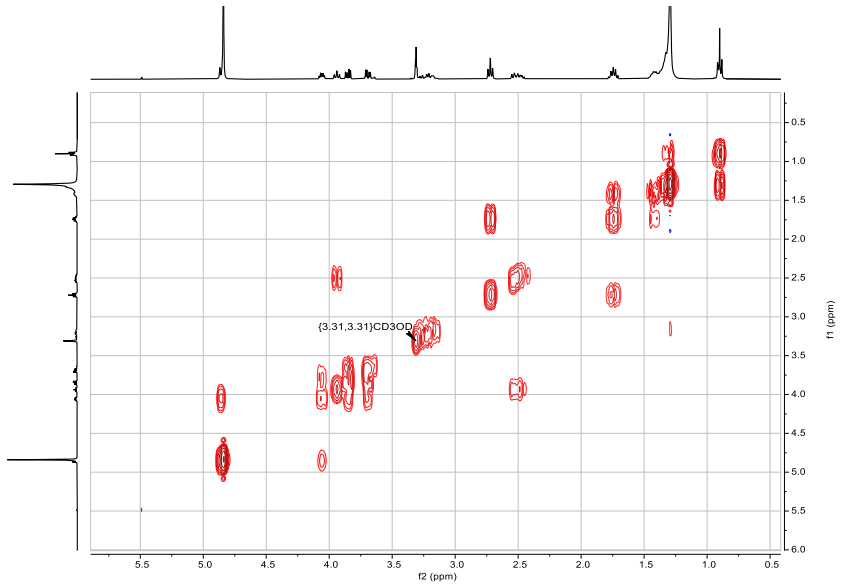


***Figure 19:*** *COSY NMR spectrum of* ***PR280-7.***

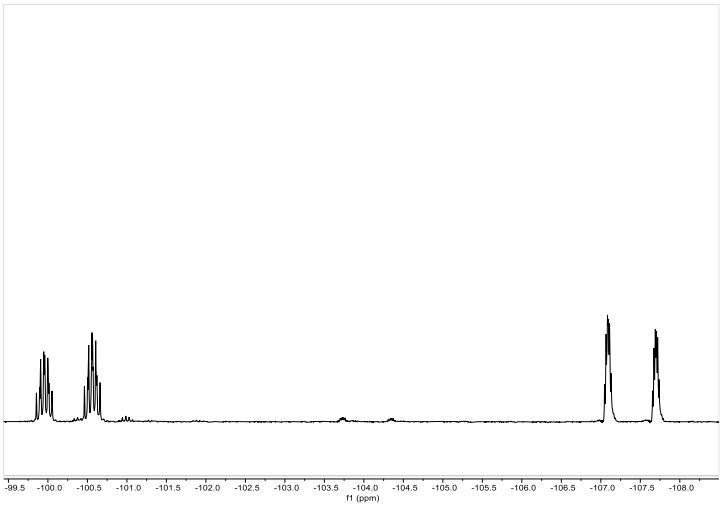


***Figure 20:*** *$^{19}$F NMR spectrum of* ***PR280-7.***

**PR280-1Boc:**

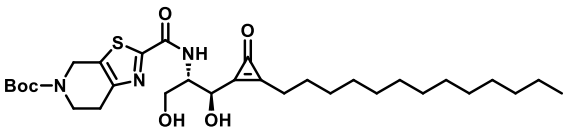


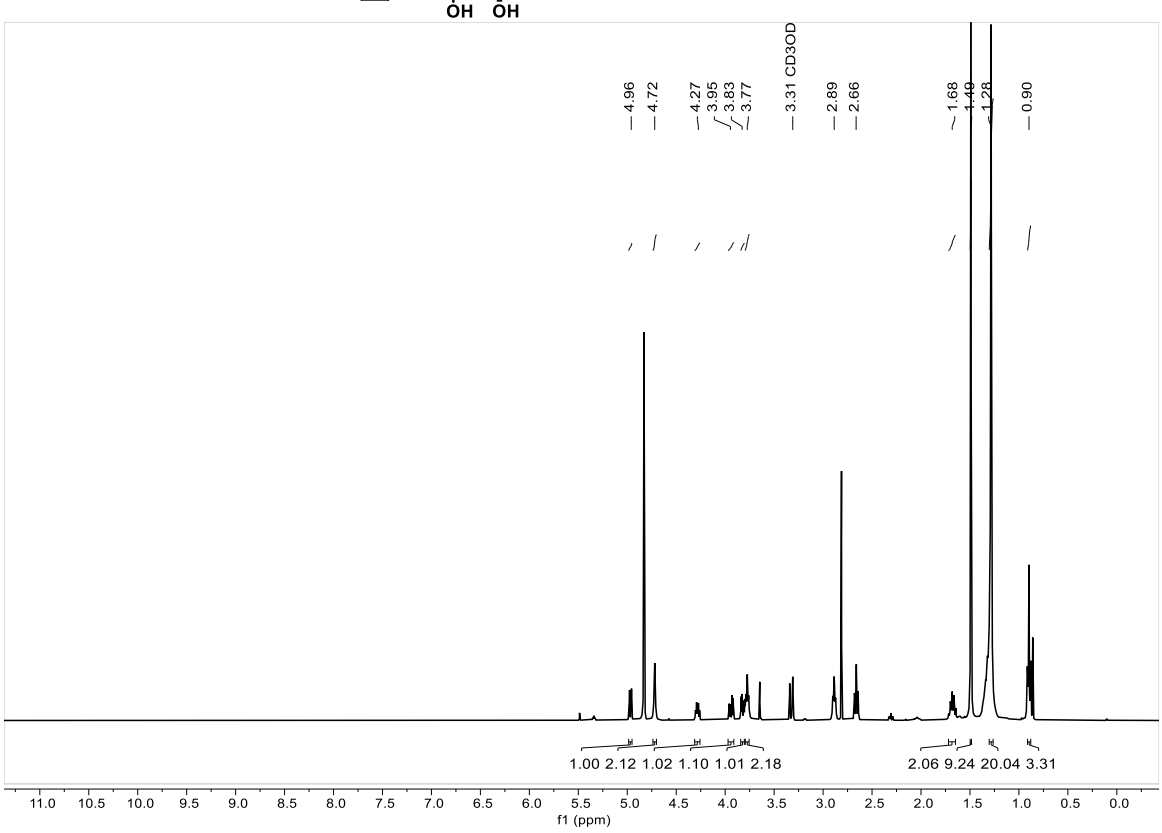


***Figure 21:*** *$^{1}$H NMR spectrum of* ***PR280-1Boc.***

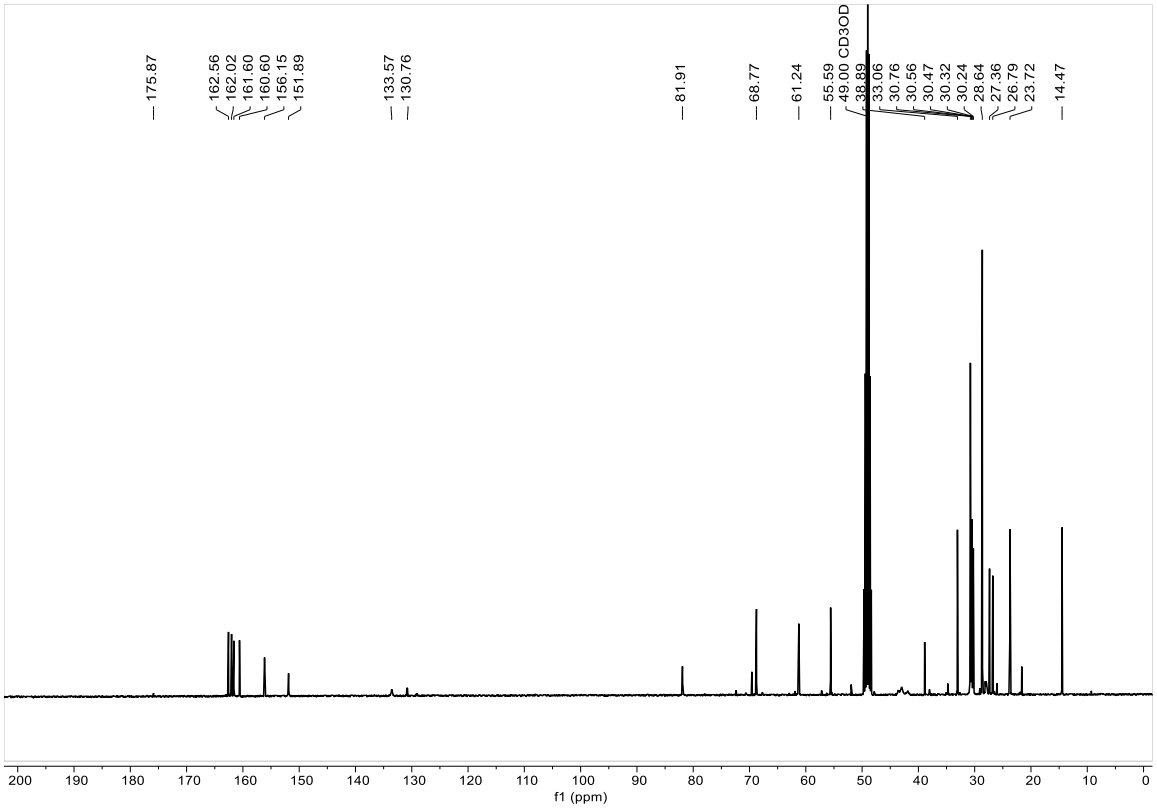


***Figure 22:*** *$^{13}$C NMR spectrum of* ***PR280-1Boc.***

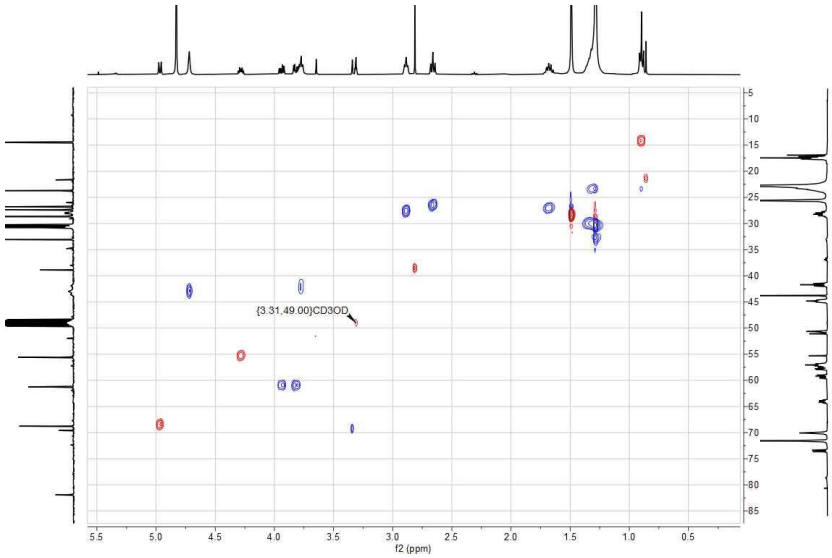


***Figure 23:*** *HSQC NMR spectrum of* ***PR280-1Boc.***

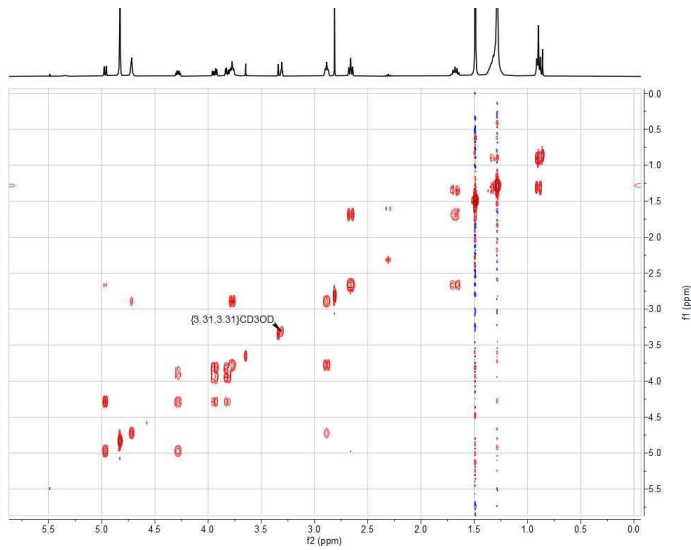


***Figure 24:*** *COSY NMR spectrum of* ***PR280-1Boc.***

**PR280-1:**

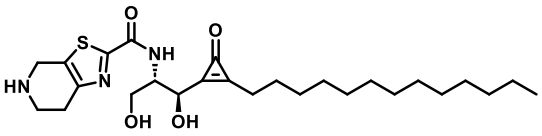


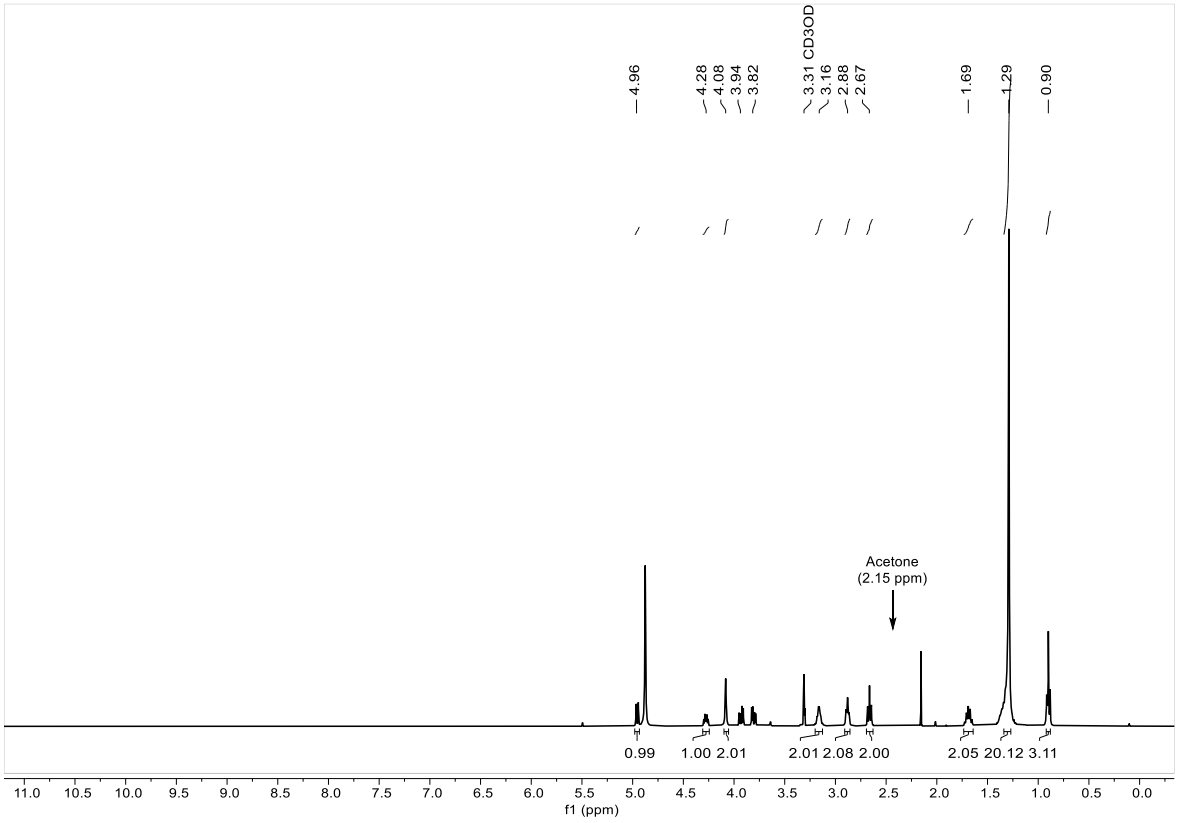


***Figure 25:*** *$^{1}$H NMR spectrum of* ***PR280-1.***

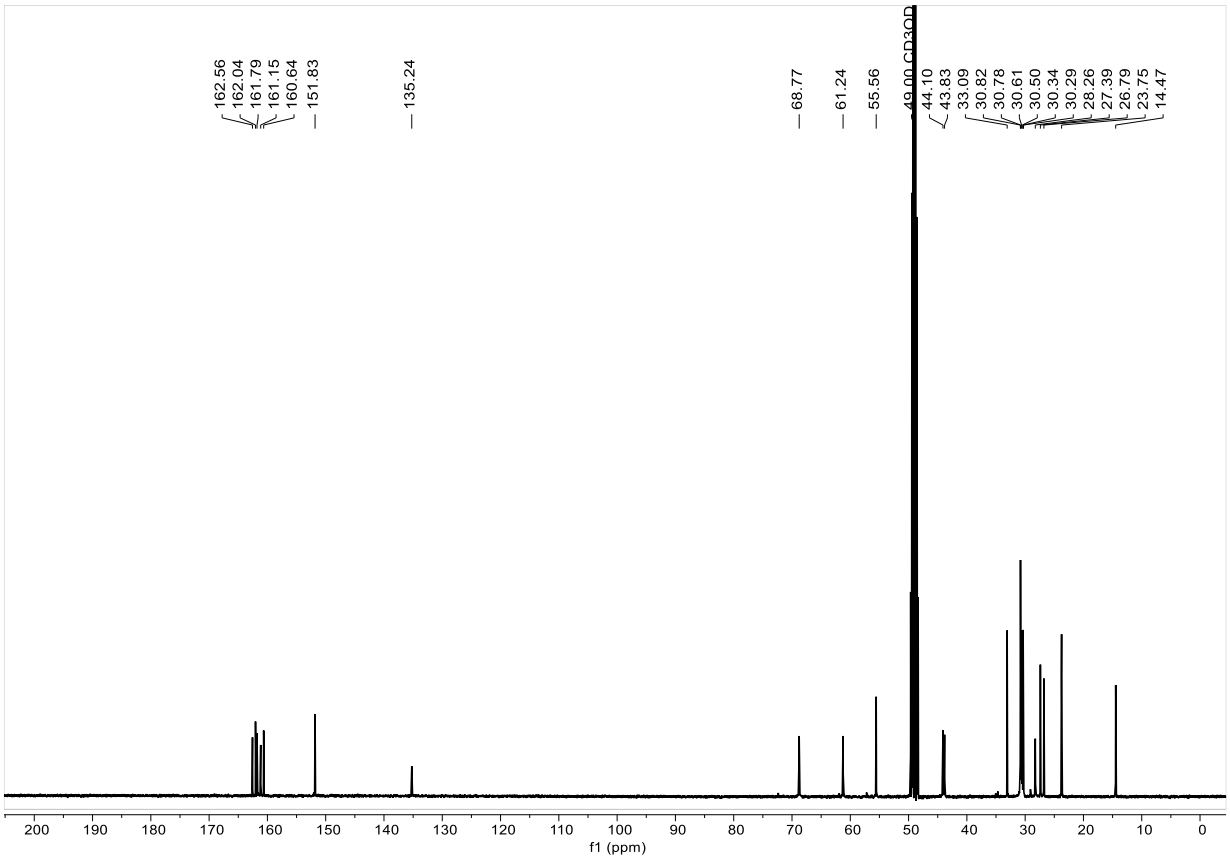


***Figure 26:*** *$^{13}$C NMR spectrum of* ***PR280-1.***

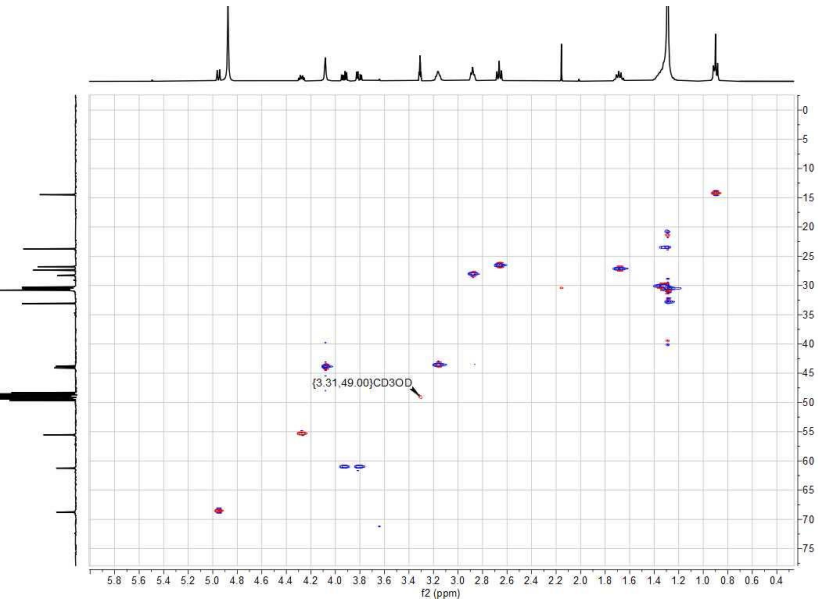


***Figure 27:*** *HSQC NMR spectrum of* ***PR280-1.***

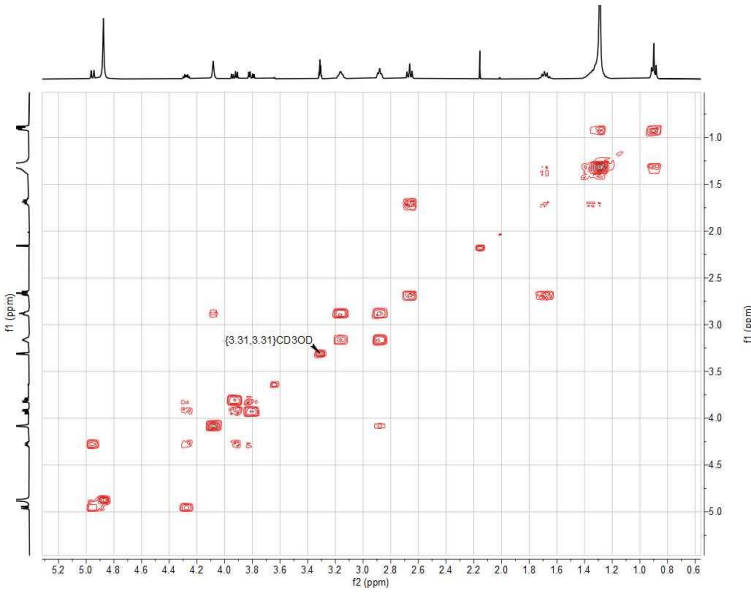


***Figure 28:*** *COSY NMR spectrum of* ***PR280-1.***

**PR280-3:**

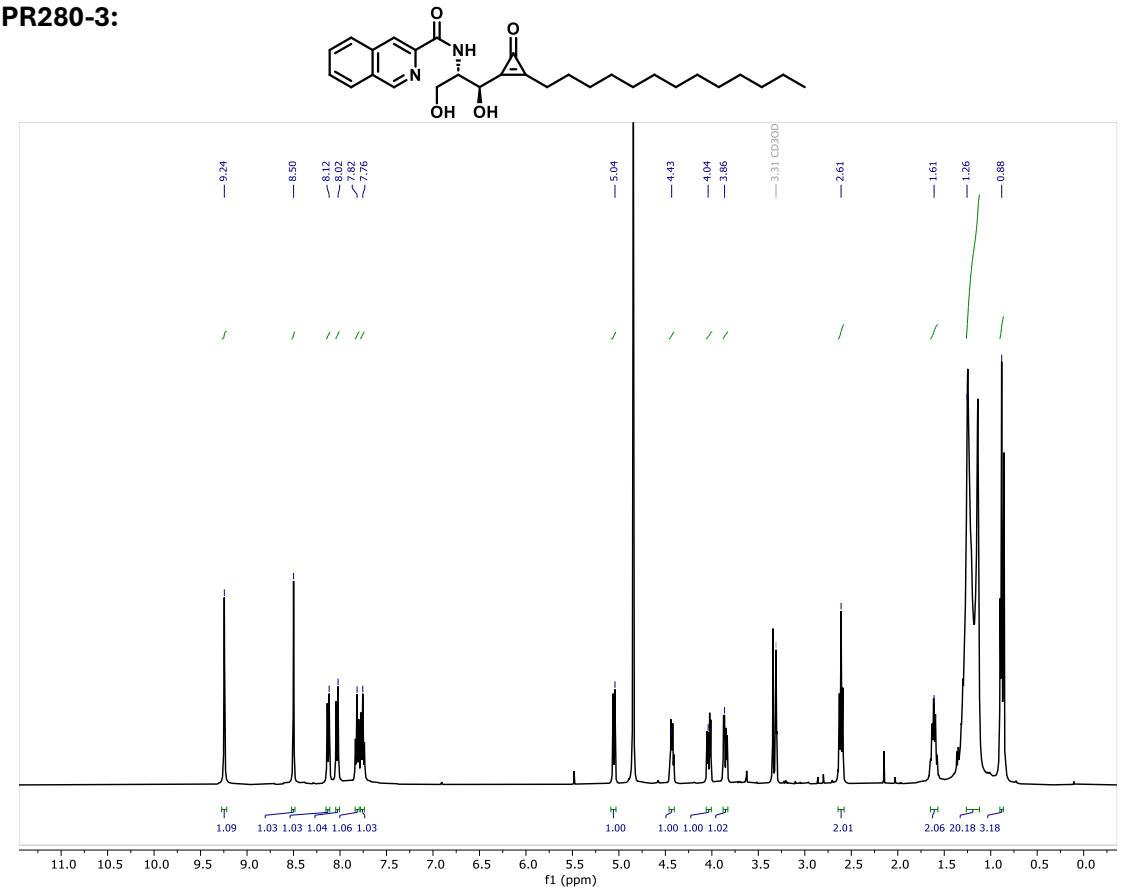


***Figure 29:*** *$^{1}$H NMR spectrum of* ***PR280-3.***

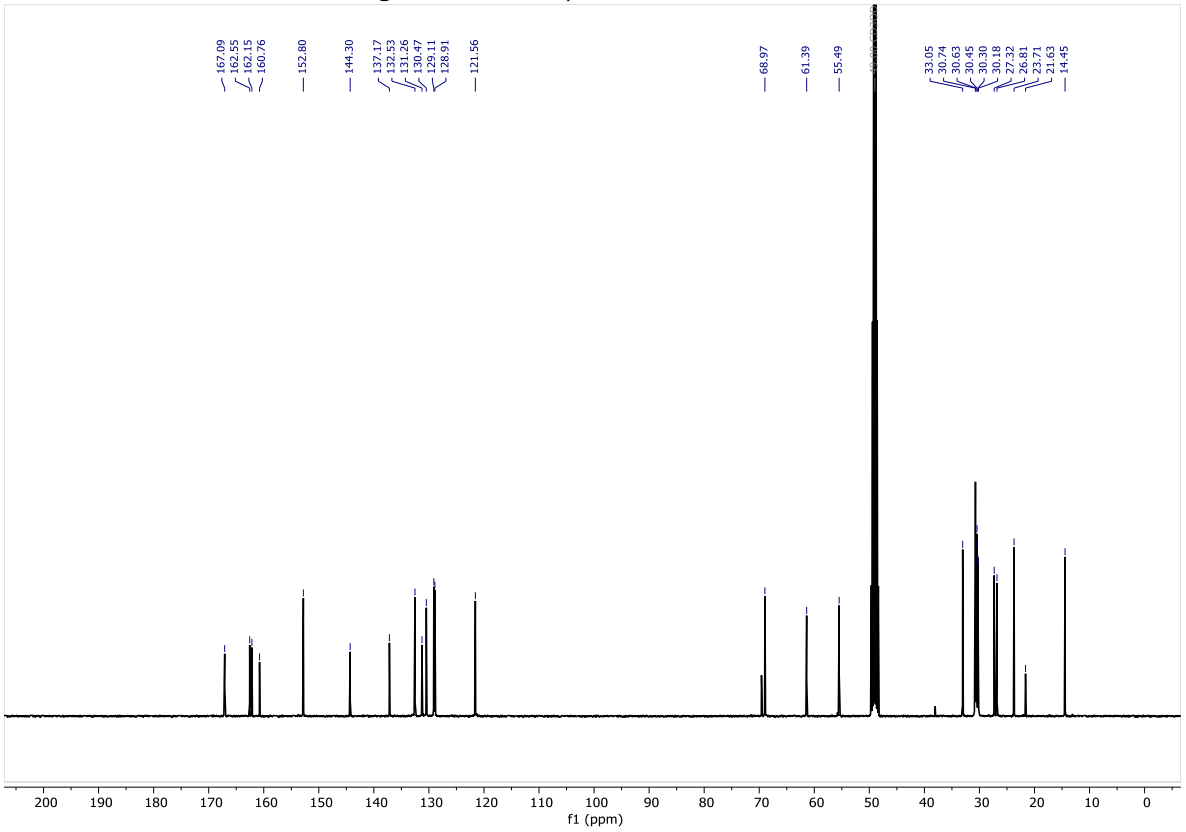


***Figure 30:*** *$^{13}$C NMR spectrum of* ***PR280-3.***

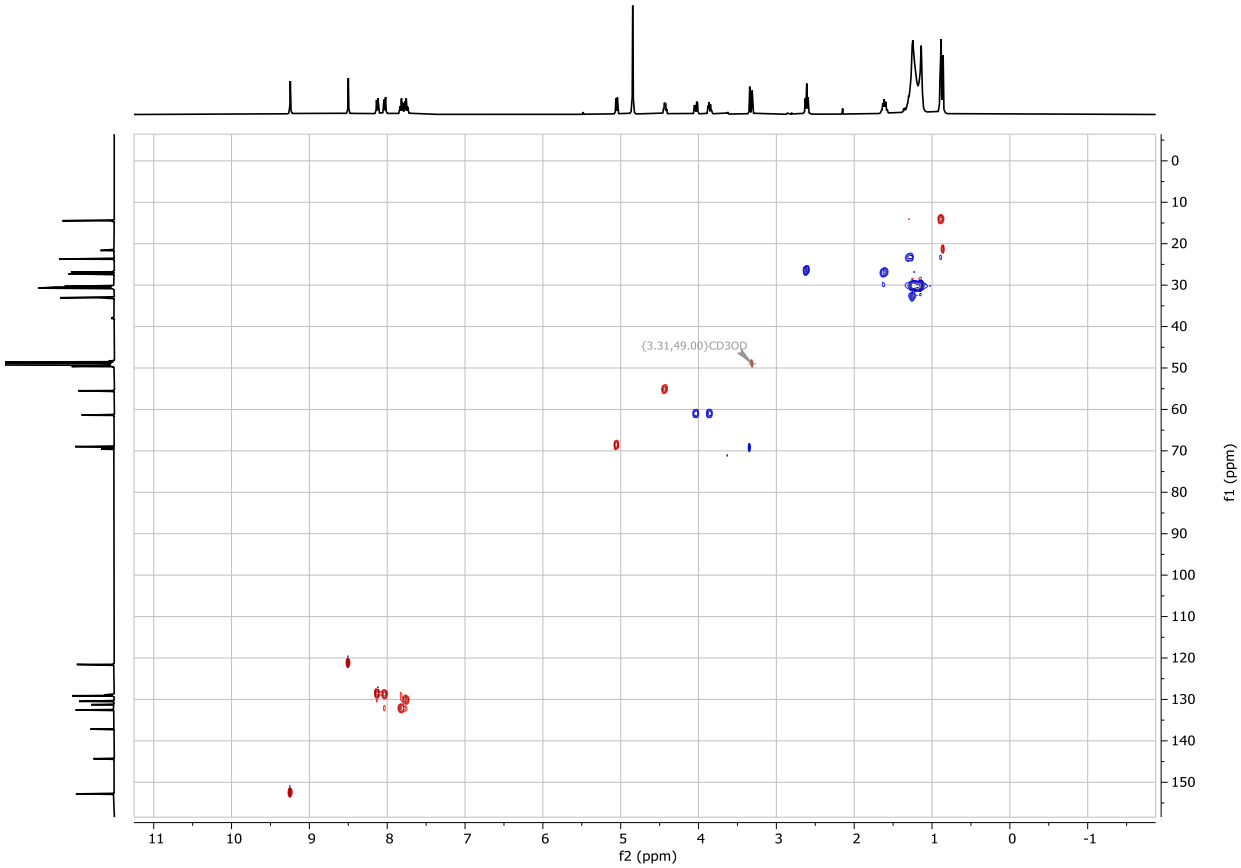


***Figure 31:*** *HSQC NMR spectrum of* ***PR280-3.***

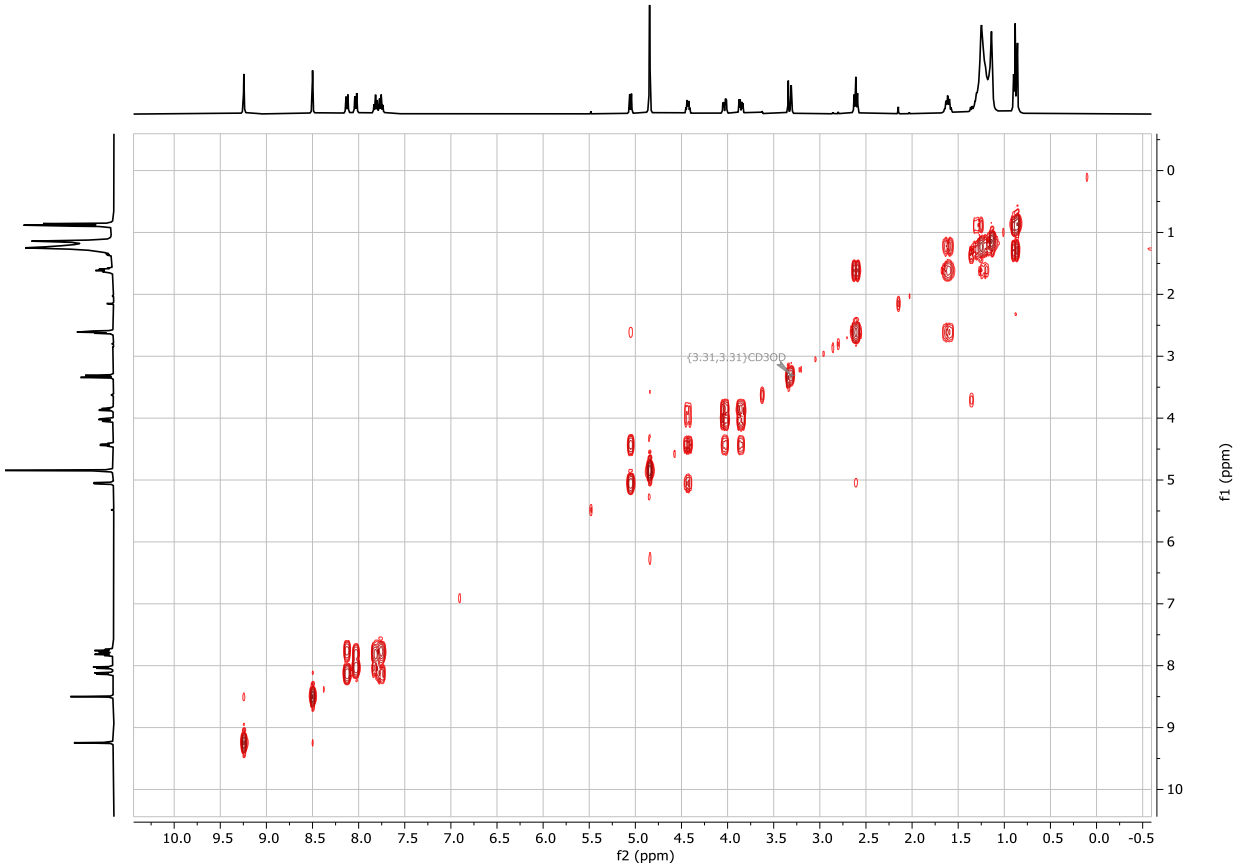


***Figure 32:*** *COSY NMR spectrum of* ***PR280-3***